M. Sc. Thesis
Meteorology

ASSESSING POLLUTANT VENTILATION IN CITY PLANNING ALTERNATIVES USING A LARGE EDDY SIMULATION

Mona Kurppa

3.10.2016

Supervisors: Doc. Leena Järvi, Dr Mikko Auvinen,
Doc. Antti Hellsten and Prof. Timo Vesala

Reviewers: Doc. Leena Järvi and Prof. Timo Vesala

UNIVERSITY OF HELSINKI
DEPARTMENT OF PHYSICS

P.O. BOX 64 (Gustaf Hällströmin katu 2)
FIN-00014 Helsingin yliopisto

HELSINGIN YLIOPISTO — HELSINGFORS UNIVERSITET — UNIVERSITY OF HELSINKI

Tiedekunta/Osasto — Fakultet/Sektion — Faculty	Laitos — Institution — Department
Faculty of Science	Department of Physics

Tekijä — Författare — Author
Mona Kurppa

Työn nimi — Arbetets titel — Title
Assessing pollutant ventilation in city planning alternatives using a large-eddy simulation

Oppiaine — Läroämne — Subject
Meteorology

Työn laji — Arbetets art — Level	Aika — Datum — Month and year	Sivumäärä — Sidoantal — Number of pages
Master's thesis	October 2016	62

Tiivistelmä — Referat — Abstract

This thesis is a case study of the impact of urban planning on local air quality along a planned city boulevard in western Helsinki. The aim of this study is to analyse ventilation and dispersion of traffic-related air pollutants inside street canyons and courtyards in four alternative city block design versions. In particular, whether the format and variation of building height can improve air quality in future planned neighbourhoods and as such, help improve the decision-making process in city planning.

The study employs a large-eddy simulation (LES) model PALM with embedded Lagrangian stochastic particle and canopy models to simulate transport of pollutants (air parcels) and the aerodynamic impact of street trees and a surrounding forest on pollutant transport. The embedded models are revised by the author to take into account the horizontal heterogeneity of the particle sources and plant canopy. Furthermore, three-dimensional two-way self-nesting is used for the first time in PALM in this study. High-resolution simulations are conducted over a real urban topography under two contrasting meteorological conditions with neutral and stable stratification and south-western and eastern wind direction, respectively.

The comparison of the different boulevard-design versions is based on analysing the temporal mean particle concentrations, the turbulent vertical particle flux densities and the particle dilution rate. Differences in flux densities between the versions show a strong dependence on urban morphology whereas the advection-related dilution rate depends on the volume of unblocked streamwise street canyons. A suggestive ranking of the versions is performed based on the horizontal mean values of the analysis measures (separately for the boulevard, the other street canyons, the courtyards and the surroundings). Considering both meteorological conditions, the design version with variable building height and short canyons along the boulevard outperforms the other design versions based on the ranking. This is especially pronounced in stable conditions. Surprisingly, variability in building shape did not induce clear improvements in ventilation.

This is the first high-resolution LES study conducted over a real urban topography applying sophisticated measures to assess pollutant dispersion and ventilation inside street canyons and courtyards.

Avainsanat — Nyckelord — Keywords
large-eddy simulation, urban meteorology, ventilation, air quality

Säilytyspaikka — Förvaringsställe — Where deposited
Kumpula Science Library

Muita tietoja — övriga uppgifter — Additional information

HELSINGIN YLIOPISTO — HELSINGFORS UNIVERSITET — UNIVERSITY OF HELSINKI

Tiedekunta/Osasto — Fakultet/Sektion — Faculty	Laitos — Institution — Department
Matemaattis-luonnontieteellinen	Fysiikan laitos

Tekijä — Författare — Author
Mona Kurppa

Työn nimi — Arbetets titel — Title

Assessing pollutant ventilation in city planning alternatives using a large-eddy simulation

Oppiaine — Läroämne — Subject
Meteorologia

Työn laji — Arbetets art — Level	Aika — Datum — Month and year	Sivumäärä — Sidoantal — Number of pages
Pro gradu -tutkielma	Lokakuu 2016	62

Tiivistelmä — Referat — Abstract

Tässä pro gradu -työssä tutkittiin kaupunkisuunnittelun vaikutusta paikalliseen ilmanlaatuun Helsingin yleiskaavassa 2050 nykyiselle Hämeenlinnanväylälle suunnitteilla olevalla kaupunkibulevardilla kaupungin länsiosassa. Tavoitteena oli verrata liikenteen päästöjen kulkeutumista ja tuulettumista pois katukuiluista ja sisäpihoilta käyttäen neljää erilaista kaupunkikorttelimalli, ja tutkia voiko rakentamisratkaisuilla parantaa ilmanlaatua.

Tutkimus tehtiin käyttäen suurten pyörteiden simulaatiomallia (large-eddy simulation, LES) PALM. Lisäksi malliin on liitetty Lagrangelainen stokastinen hiukkasmalli, jolla simuloitiin hiukkasten (ilmapakettien) kulkeutumista ilmavirtauksen mukana, sekä kasvillisuusmalli, joka huomioi katupuiden ja läheisen metsän aerodynaamisen vaikutuksen ilmanvirtaukseen ja näin ollen myös hiukkasten kulkeutumiseen. Tutkimusta varten hiukkas- ja kasvillisuusmalleja kehitettiin ottamaan huomioon sekä hiukkaslähteiden että puiden sijainnin horisontaalisen vaihtelevuuden. Lisäksi mallisimulaatioissa hyödynnettiin ensimmäistä kertaa ominaisuutta, jossa ison laskenta-alueen sisällä on määritelty pienempi ja tiheähilaisempi laskenta-alue, mahdollistaen samanaikaisesti sekä suuren laskenta-alueen että riittävän laskentaerotuskyvyn. Mallisimulaatiot tehtiin todellisen kaupunkitopografian yllä käyttäen korkeaa laskentaerotuskykyä kahdessa eri säätilanteessa, neutraalisti ja stabiilisti kerrostuneelle rajakerrokselle lounais- ja itätuulella.

Eri kortteliversioita arvioitiin tarkastelemalla keskimääräisiä hiukkaspitoisuuksia, turbulenttista pystysuuntaista hiukkasvuotieheyttä sekä hiukkaspitoisuuksien laimenemisnopeutta. Erot hiukkasvuotiheyden voimakkuudessa määräytyivät rakennusten muodon ja orientaation mukaan, kun taas laimenemisnopeus riippui virtauksen esteettömyydestä. Kortteliversiot luokiteltiin laskemalla analyysimuuttujien aluekeskiarvot erikseen bulevardille, muille katukuiluille, sisäpihoille ja ympäristölle, ja asettamalla kortteliversiot paremmuusjärjestykseen kaikkien muuttujien perusteella. Molemmat meteorologiset olosuhteet huomioiden, korttelimalli vaihtelevalla rakennuskorkeudella ja suurella määrällä risteyksiä bulevardia pitkin osoittautui luokittelun mukaan parhaaksi vaihtoehdoksi. Tämä havaittiin etenkin stabiilissa säätilanteessa, joka yleensä johtaa huonoon ilmanlaatuun Helsingissä. Yllättäen, rakennusmuodon vaihtelevuus ei osoittanut voimistavan tuulettumista.

Tämä on ensimmäinen todellisen kaupunkitopografian yllä suoritettu korkean laskentaresoluution LES-tutkimus, jossa päästöjen kulkeutumista ja tuulettumista arvioidaan käyttäen useita suoria ja aiempaa monimutkaisempia mittareita. Tuloksia tullaan hyödyntämään kaupunkisuunnittelussa ja päätöksenteon tukena, kun tavoitteena on rakentaa mahdollisimman puhtaita elinympäristöjä.

Avainsanat — Nyckelord — Keywords
large-eddy simulation, kaupunkimeteorologia, tuulettuminen, ilmanlaatu

Säilytyspaikka — Förvaringsställe — Where deposited
Kumpulan tiedekirjasto

Muita tietoja — övriga uppgifter — Additional information

Contents

1 Introduction

Urban areas are commonly suffering from elevated pollutant emission levels owing to high traffic rates in particular. Likewise, over half of the World's population lives in urban areas (United Nations, 2014) and the majority of them reside at pedestrian level where exposure to air pollution can have several detrimental health effects. Most injurious pollutants include fine particulate matter, ozone and nitrogen dioxide, which cause respiratory and cardiovascular diseases and increase mortality (Brunekreef and Holgate, 2002; Pope and Dockery, 2006; McCreanor et al., 2007). As an example, around 3.7 million premature deaths worldwide in 2012 were linked to exposure to elevated concentrations of fine particulate matter according to the World Health Organization (WHO, 2012).

Busy streets are often flanked by buildings as well as street trees. These obstacles strongly modify the air flow over an urban surface, which further alters pollutant transport and ventilation, i.e. replacement of polluted air by fresh air (e.g. Britter and Hanna, 2003). As a result, pollutants can be retained close to their source and largest pollution levels are generally observed at pedestrian level inside street canyons (e.g. Yazid et al., 2014). Moreover, polluted air can also enter buildings and decrease indoor air quality (e.g. Weschler and Shields, 2000). Therefore, urban planning is one the key factors in local urban air quality.

In 2014, the City Planning Department of Helsinki published an outline of the City Plan for 2050 (City Planning Department, City of Helsinki, 2015). One of the key elements of the plan is to urbanise the city northwards from the city centre by transforming the motorway-like entry routes in the outer suburbs into urban 'city boulevards'. These boulevards would be framed by densely built neighbourhoods with business premises and shops at ground floor level. Ensuring a liveable and healthy urban environment in the proximity of any boulevard sets requirements on both the traffic system and apartment block structures. Local traffic emissions are expected to decrease along with the boulevardisation, which encourages walking, cycling and the use of public transport. Future technological developments are seen likely to support the aims. Furthermore, there is discussion taking place within the City Council as to whether congestion road tolls should be introduced as a calming measure for private cars in the future. However, the expected decrease in the local emission levels may occur gradually. Hence, understanding pollutant transport and maximizing ventilation of street canyons and courtyards by means of a proper city block design is essential for ensuring a good air quality in a densely built neighbourhood.

Characteristics of the flow field and the pollutant transport processes over an urban surface have been widely studied by means of wind-tunnel simulations (e.g.

Nosek et al., 2016), field measurements (Idczak et al., 2007) and computational fluid dynamics (CFD) simulations using either large-eddy simulation (LES) models (e.g. Liu et al., 2005) or models based on the Reynolds-averaged Navier-Stokes (RANS) equations (e.g. Liu et al., 2011). CFD models outrage wind tunnel simulations and field measurements as they provide with a complete three dimensional flow field and have controlled conditions without any similarity constraints (Ramponi et al., 2015; Giometto et al., 2016). Most of the urban CFD studies have applied RANS owing to lower computational costs, despite LES has been found to outperform above an urban surface (e.g. Letzel et al., 2008; Tominaga and Stathopoulos, 2011; Yazid et al., 2014; Giometto et al., 2016) also when including street trees (Salim et al., 2011b).

Majority of the previous LES studies on ventilation have been conducted over an idealistic two-dimensional street canyon or a very simplified urban topography without including the impact of street trees (e.g. Baik and Kim, 2002; Cai et al., 2008; Li et al., 2009). However, wind flow and pollutant dispersion have been found to have more complex structures over a group of buildings (e.g. Kanda et al., 2013; Gousseau et al., 2015) or inside a street canyon including street trees (e.g. Gu et al., 2010; Salim et al., 2011a). A small number of LES studies have been conducted over a real urban surface but often the scope has been only on the flow field (Nozu et al., 2008; Letzel et al., 2008; Kanda et al., 2013; Park et al., 2015a) or pollutant concentrations without further investigations on pollutant ventilation (Tamura, 2008; Xie and Castro, 2009; Zheng et al., 2015). The few ventilation studies conducted over a real urban topography (Letzel et al., 2012; Keck et al., 2014; Park et al., 2015b) have only applied a simple, indirect ventilation indicator, velocity ratio $v_r = v_p/v_\infty$, i.e. the ratio between the wind velocities at $z = 2$ m above ground level and at the top of the model domain, respectively. Furthermore, previous studies on the ventilation of courtyards are scarce (Moonen et al., 2011; Padilla-Marcos et al., 2016).

In this study, pollutant ventilation and dispersion inside street canyons and courtyards are being investigated for four different city block design versions. The study site on Hämeenlinnanväylä in western Helsinki is one of the planned city boulevards in the City Plan for 2050. The turbulent wind field and pollutant transport are simulated over a real urban topography using a LES model coupled with a Lagrangian stochastic particle model. Furthermore, the aerodynamic impact of street trees and a surrounding forest on pollutant transport is included by means of an embedded plant canopy model. The study is conducted using two different meteorological conditions in order to rule in the relative impact of weather conditions on pollutant transport. Ventilation and dispersion are assessed by means of three different measures to give insight into the relative

performance of each design version when it comes to providing with a good local air quality. The aim of the study is to compare pollutant ventilation and dispersion in four alternative boulevard design versions, and to provide important information about the impact of urban planning on local air quality. This is a practical study that applies an accurate and detailed high-resolution wind flow and pollutant dispersion modelling methodology in urban planning and decision making.

2 Theory and background

2.1 Planetary boundary layer

The planetary boundary layer (PBL), also called the atmospheric boundary layer (ABL), is the lowest layer of the troposphere where the flow field is directly influenced by interactions with the Earth's surface with a response time of one hour or less (Stull, 1988; Holton, 1992). Ultimately, the interactions are governed by molecular viscosity, which is relevant only within a few millimetres above the surface in the viscous sublayer. Nevertheless, molecular viscosity results in no-slip conditions at ground, generating wind shear and frictional drag (Holton, 1992). Frictional drag together with buoyancy near the surface produce turbulence, which in turn results in exchange of energy, momentum and mass between the surface and the PBL. The turbulent nature of the PBL separates it from the rest of the atmosphere. The height of the PBL varies with time and space as it depends on the strength of the surface generated mechanical and thermal turbulent mixing. For instance, on a sunny day with strong and an unstable stratification the depth of the PBL may extend to 2 km whereas on a clear cold night a downward heat flux increases stability and may reduce the PBL depth to a few tens of meters (Oke, 1987).

The lowest 5 - 10 % of the PBL is called the surface layer (Oke, 1987; Foken, 2008), where the interaction is strongest. In the surface layer, the impact of frictional forces exceeds that of Coriolis force which is commonly neglected. The wind profile is adjusted to have a nearly constant direction and an approximately logarithmically increasing speed with height. The surface layer is further divided into an inertial sublayer and a roughness sublayer, which will be discussed in Section 2.2.1. Above the surface layer up to the PBL height lies a layer which is called an Ekman layer, a daytime mixing layer or a nocturnal boundary layer, depending on the stratification and driving forces. Here, the wind speed is nearly constant but the wind direction turns counter-clockwise towards the surface (Holton, 1992). The PBL is separated from the free atmosphere aloft by

a statically-stable entrainment zone with intermittent turbulence. All exchange processes between the PBL and free atmosphere aloft take place in this layer with a thickness of around 10 % of the PBL depth (Foken, 2008).

2.1.1 Turbulence

As mentioned, the dominant feature of the PBL is turbulence, which is irregular three-dimensional fluctuation of a fluid. Fluctuations have wide continuous spectrum of both spatial and temporal scales, which leads to efficient mixing of mass and fluid properties. Vertical and horizontal scales of turbulent eddies are of the same order of magnitude. The maximum extent of turbulent eddies is set by the depth of the boundary layer whereas the diffusion by molecular friction limits the minimum spatial scale to 10^{-3} m (Holton, 1992). Turbulent eddies account for the direct interaction between the surface and air, and maintain the energy and momentum balances at the surface (Holton, 1992). Simulation of turbulence is challenging since the equations describing the mean flow quantities are not closed, and therefore a statistical approach is needed (Berselli et al., 2006).

Turbulent variations are imposed on the mean flow field. Hence, according to Reynolds decomposition (Reynolds, 1895), any variable s can be decomposed into its time-average $\overline{s}$ and temporal fluctuations s', i.e.

$$s = \overline{s} + s' \tag{1}$$

so that $\overline{s'} = 0$. This is a common way to isolate turbulent variations of wind velocity, heat, humidity and any other scalar from the large-scale variations.

In the atmosphere, turbulence is produced either thermally or mechanically. On a sunny day, solar heating destabilizes the surface air, which generates positive buoyancy and thermals of warm air, i.e. large eddies. Similarly, stability can suppress turbulence in stable conditions for example during a clear night. Mechanical production arises from wind shear or deflection of flow by obstacles. Wind shear is produced by frictional drag as air flows over a surface. Shear can produce dynamic instabilities, which results in a turbulent flow. An obstacle in turn generates turbulent wakes downwind (Stull, 1988).

Turbulent kinetic energy (TKE) is the part of the kinetic energy contained by turbulent motions, and it is one of most important quantities to describe turbulence. Mean turbulent kinetic energy per unit mass (e) over a certain time period is defined

$$\overline{e} = (\overline{u'}^2 + \overline{v'}^2 + \overline{w'}^2)/2\,, \tag{2}$$

where $\overline{u'}^2$, $\overline{v'}^2$ and $\overline{w'}^2$ are the time-averaged variances of each three velocity

component (Stull, 1988). TKE is produced by conversion of energy from the mean flow to turbulent fluctuations. The time-averaged TKE budget equation can be derived from the prognostic equation (see Equation 4) as follows

$$\frac{\partial \overline{e}}{\partial t} = -\overline{u_j}\frac{\partial \overline{e}}{\partial x_j} + \delta_{i3}\frac{g}{\overline{\theta_v}}\left(\overline{u_i'\theta_v'}\right) - \overline{u_i'u_j'}\frac{\partial \overline{u_i}}{\partial x_j} - \frac{\partial\left(\overline{u_j'e'}\right)}{\partial x_j} - \frac{1}{\overline{\rho}}\frac{\partial\left(\overline{u_i'p'}\right)}{\partial x_i} - \epsilon, \tag{3}$$

where $\{i, j, k\} \in \{1, 2, 3\}$, and thus u_i are the velocity components ($u_1 = u$, $u_2 = v$ and $u_3 = w$) and x_i are the Cartesian coordinates ($x_1 = x$, $x_2 = y$ and $x_3 = z$). Moreover, g is the gravitational acceleration, θ_v is the virtual potential temperature, ρ is the air density, p is the atmospheric pressure and δ_{ij} is the Kronecker delta function. From the left the terms in Equation 3 are called the tendency, the advection, the buoyant production or loss, the shear production, the turbulent transport, the pressure correlation and the dissipation. TKE flows towards smaller eddies due to vortex stretching and twisting, and TKE is constantly dissipated into heat by viscous diffusion of the smallest eddies. Thus, continuous production of turbulence is needed to maintain TKE (Holton, 1992).

2.1.2 Equations of motion

The Navier-Stokes equation describes motion of a viscous fluid. For an incompressible, Newtonian fluid, the equation can be written (Stull, 1988)

$$\frac{\partial u_i}{\partial t} = -u_j\frac{\partial u_i}{\partial x_j} - \frac{1}{\rho}\frac{\partial p}{\partial x_i} - \delta_{i3}g - \epsilon_{ij3}f_c u_j + \nu\frac{\partial^2 u_i}{\partial x_j^2}. \tag{4}$$

Here, $f_c = 2\Omega\sin(\phi)$ is the Coriolis parameter, where Ω is the angular velocity of the Earth and ϕ is the latitude. Furthermore, ν is the kinematic viscosity and ϵ_{ijk} is the three-dimensional Levi-Civita symbol defined as

$$\epsilon_{ijk} = \begin{cases} 1 & \text{for} \quad ijk = 123, 231 \text{ or } 312 \\ -1 & \text{for} \quad ijk = 321, 213 \text{ or } 132 \\ 0 & \text{for any two or more equal indices.} \end{cases} \tag{5}$$

From the left, the terms in Equation 4 are called the tendency, the advection, the pressure gradient force, the gravitational acceleration, the Coriolis force and the molecular (viscous) stress. In the PBL, all terms have to be included when solving a turbulent wind field explicitly (Foken, 2008). Turbulent eddies can have large values of shear in localized eddy-size regions and thus viscosity should not be neglected when forecasting turbulence (Stull, 1988).

2.2 Urban boundary layer

Each local land cover type generates an internal boundary layer when air flows over it. Inside the internal boundary layer, the flow structure and the vertical profiles of temperature, humidity and mass concentration adjust to the specific surface characteristics. The vertical profiles are advected with a nearly horizontal wind field forming a layer of discontinuity and also resulting in transport of heat, moisture and scalars up to hundreds of kilometres downstream (Foken, 2008; Stull, 1988). The height of the internal boundary layer increases with increasing fetch at a rate relative to the surface roughness and atmospheric stability (Oke, 2006).

An urban boundary layer (UBL) develops downwind from the leading edge of urban areas (see Figure 1a). The characteristics of the UBL are governed by the urban surface. The urbanization has led to modifications in the radiative, thermal, moisture and aerodynamics characteristics of natural surfaces, making them rougher, warmer and usually also drier than rural surfaces (Oke, 1987; Arya, 2001).

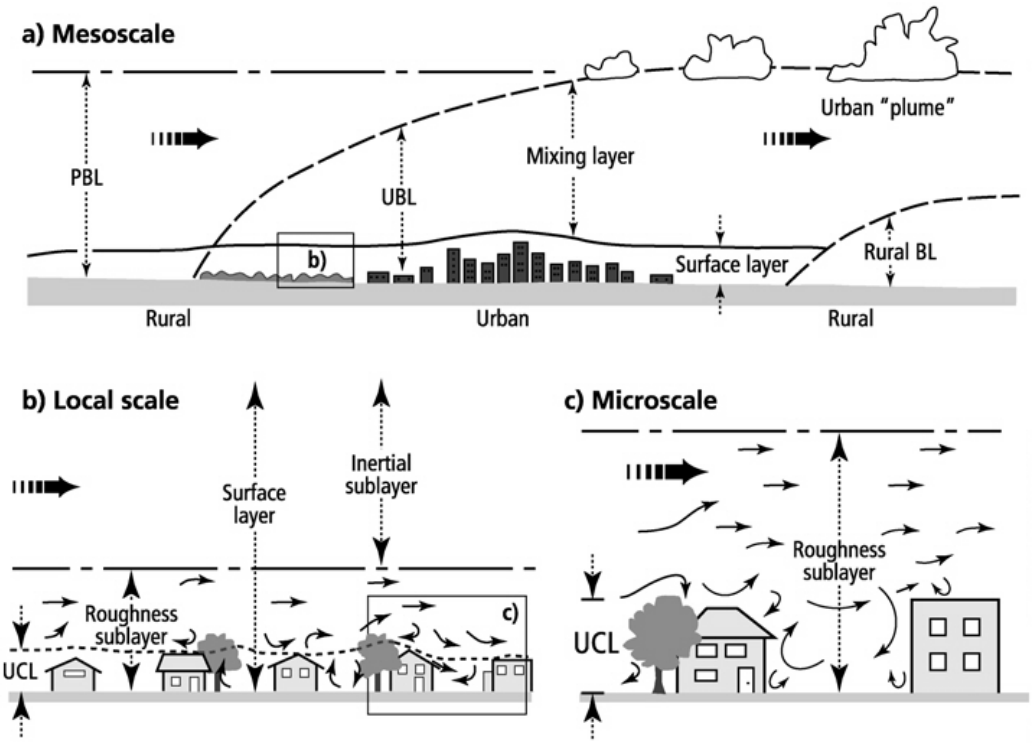

Figure 1: Schematic of the vertical and horizontal layers and scales within an urban boundary layer (UBL). PBL stands for the planetary boundary layer, BL for a boundary layer and UCL for the urban canopy layer (Oke, 2006, Figure 1).

The flow inside the UBL is modified both by increased roughness and heat. Firstly, buildings are the most important roughness elements deflecting the flow over a city both vertically and horizontally. Enhanced aerodynamic roughness

increases the surface drag and generates mechanical turbulence. Secondly, urban areas can become notably warmer than their surrounding rural areas mainly due to changes in radiative fluxes as buildings block and reflect radiation, and also owing to an elevated anthropogenic waste heat release resulting from additional heat input by human activities (Souch and Grimmond, 2006). This phenomenon of local warming is called the urban heat island (UHI) (Oke, 1973). As a result, increased heat fluxes at the surface due to UHI generate thermal turbulence. In addition, air flowing from slightly colder surrounding rural regions over an urban area is decelerated by the increased surface drag, which can lead to wind convergence and convection.

The increased surface drag together with the UHI effect and the convergence-initiated convection maintain the vertical turbulent mixing in the UBL. Thus, no strong temperature gradients or stratification are typically observed over an urban area. Turbulent mixing is enhanced even at night. This increases the wind speeds at the surface, which prevents formation of strong inversions and poor air quality events especially in high latitude cities (Oke, 1987).

2.2.1 Scales and layers

Urban boundary layer is generally presented using conceptual models of horizontal scales and vertical layers. Firstly, following Oke (2006), the horizontal scales of interest in the UBL are divided into micro-, local- and mesoscale. At the microscale (Figure 1c), the airflow is highly perturbed by individual objects and surfaces. Each of them produces its own microclimate around it owing to differences in construction material, angle of attack of the wind and radiative balance (Oke, 1987). The typical scales are determined by the dimensions of individual obstacles (buildings, trees, street canyons etc.), extending from less than one metre up to 100-200 m (Britter and Hanna, 2003). This study is conducted at the microscale. At the local scale (Figure 1b, also called the neighbourhood scale), urban areas are treated using the land-use classes describing the surface cover, size and spacing of buildings, and human activity. Typical scales are from a few hundred metres up to one to several kilometres, and thus the local scale represents the mixed impact of microclimatic effects. Finally at the mesoscale (Figure 1a), the impact of a city or an urban region on weather and climate is considered at its whole, and thus typical scales are up to tens of kilometres. Formation of the UBL is a mesoscale phenomenon.

The UBL has the general vertical structure of the PBL with a surface layer that is further divided into sublayers (Christen, 2005) (Figure 1). The lowest vertical layer of the UBL is the urban canopy layer (UCL), which develops between the ground and the average roof level by microscale processes in the street

canyons. In other words, the flow and the exchange processes are governed by turbulent structures generated by individual objects. In general, canopy layer winds are notably slower than in the air above but local "jets" may occur if the faster moving upper level flow is deflected downward by taller buildings or channelled along streets parallel to the wind direction (Oke, 1987). The UCL is included in the roughness sublayer (RSL), which extends from the surface up to the blending height where the impact of individual roughness elements is mixed. This blending height is generally found at 1.5–4 times the mean obstacle height (Christen, 2005). Within the RSL, the turbulence statistics are both horizontally and vertically heterogeneous, and the horizontal advection cannot be neglected. The RSL is also the layer where the human population resides and also most of the pollutant emission occur, which emphasizes the importance to understand the complex nature of the RSL (Christen, 2005). Above the blending height lies the inertial sublayer (ISL), where the flow is spatially well blended. In the ISL, the turbulent fluxes are constant with height and Monin-Obukhov similarity theory generally applies as the flow feels the urban area only as a rough surface (Oke, 2006).

2.2.2 Aerodynamic impact of solid obstacles

In an urban environment, the surface cover and roughness are altered both by planting and construction of man-made structures. Tall obstacles, like buildings and trees, strongly modify the wind field and change the aerodynamics in the boundary layer. Modifications can be both intentional and unintentional (Oke, 1987). They can provide with comfortable wind shelters but also result in an unintentionally gusty and uncomfortable environment or, the opposite, a calm environment where atmospheric pollutants could accumulate.

When air flowing over a surface encounters an obstacle, the flow is forced to change its path and the flow structure can be separated into four zones: undisturbed, displacement, cavity and wake (Figure 2, Oke (1987)). Already well before encountering the obstacle, the initially undisturbed flow (A) starts to separate from the surface of the obstacle in the displacement zone (B). Pressure builds up on the upwind wall of the obstacle and the air is forced to deflect over the top, around the sides or down the front. The downward eddy is also called the bolster eddy vortex (Oke, 1988). After passing the obstacle, the convergence of streamlines accelerates the flow until the room for expansion suddenly increases behind the obstacle. However, the flow cannot immediately adjust to the volume and separates further into wake (D) and cavity zones (C). The cavity is a highly turbulent zone formed right behind the obstacle, where the flow can be reverse to the undisturbed wind field. The inverse flow can extend to on top of the obstacle.

In the wake, the momentum transport is enhanced due to residual turbulence. Furthermore, wind speeds are increased at the horizontal ends of the obstacle due to the flow separation. How far after the obstacle does the flow remain perturbed depends on the permeability of the obstacle, and thus the impact on the wind field is different for a building than for a tree.

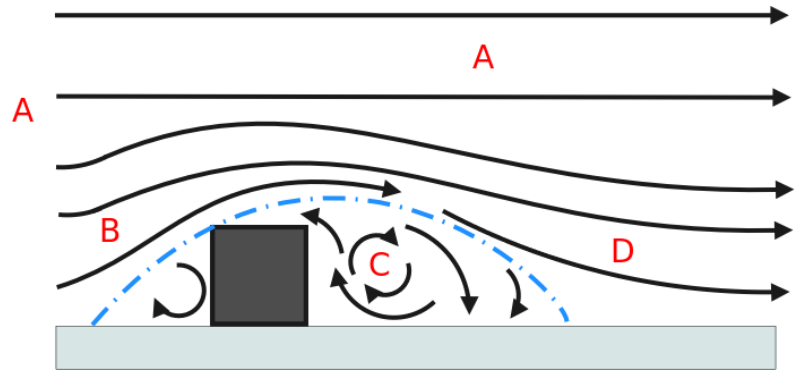

Figure 2: Schematic of different zones when an air flow encounters an obstacle. A: Undisturbed, B: Displacement, C: Cavity and D: Wake. The bolster eddy vortex and the cavity are marked with a blue dash-dot line. (Adapted from Oke (1987), Figure 8.1).

Over an urban area, the aerodynamic impact of many single obstacles is merged. When a flow encounters a system of many buildings, the joint effect depends on the relative distance of the buildings from each other. A commonly used measure to classify flow patterns in a many building system is the height to width ratio (H/W), i.e. aspect ratio, where H is the mean building height and W is the mean distance between the buildings. For widely spaced buildings ($H/W < 0.4$), the joint effect is not relevant and the flow pattern is nearly similar as for isolated single buildings (Figure 3a). This type of flow is called the isolated roughness flow. When buildings are more closely spaced ($0.4 < H/W < 0.7$), a wake of a building starts to interfere with that of the next building downstream resulting in a complicated flow pattern called the wake interference flow (Figure 3b). With an even tighter spacing ($H/W > 0.7$), the main flow begins to skim over the building tops and separates from the flow within the cavity, i.e. in the street canyon between buildings. In the street canyon, a decoupled canyon vortex is formed (Figure 3c) with recirculating velocities from $^1/_3$ to $^1/_2$ of the roof-level wind speeds (Britter and Hanna, 2003). Accordingly, the flow pattern is called the skimming flow. According to previous numerical studies, several counter rotating vortices can be formed inside narrow and deep street canyons (e.g. Liu et al., 2004 and Lee and Kim, 2009).

These three patterns in Figure 3 occur when the wind is orientated normal to the street canyons. When the wind is neither normal nor parallel to the street, the

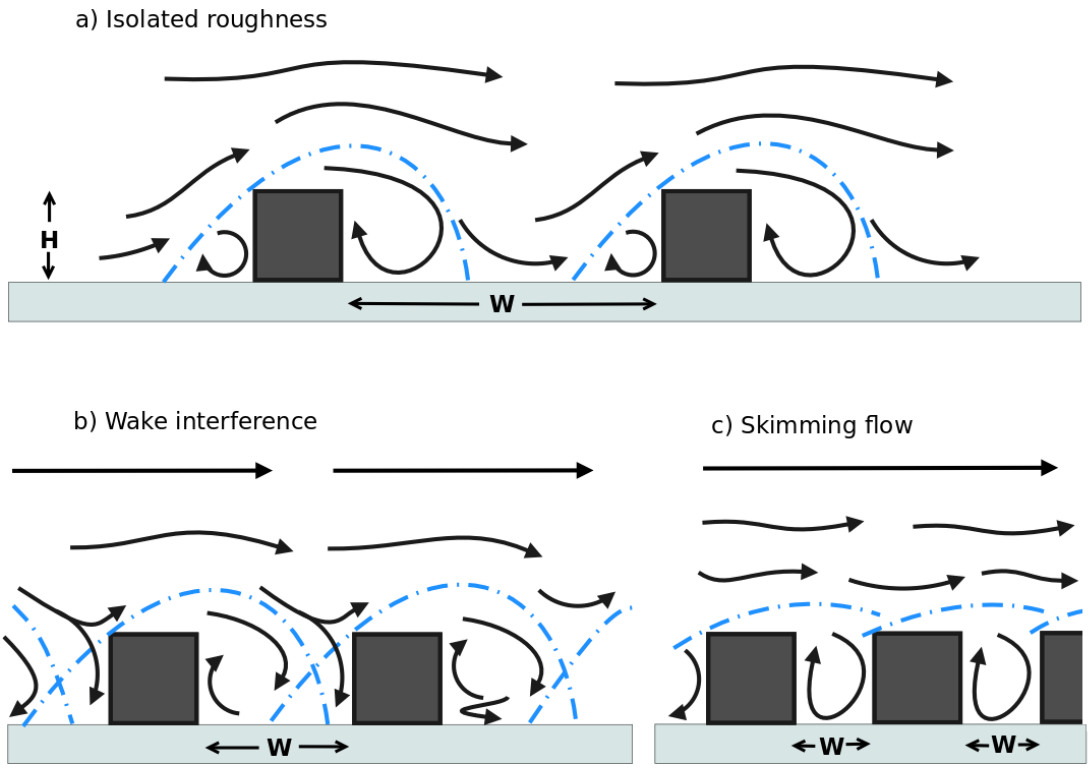

Figure 3: Schematic of flow regimes associated with air flowing over many single buildings with different aspect ratios H/W. The bolster eddy vortex and cavity of each obstacle are marked with a blue dash-dot line. (Adapted from Oke (1988), Figure 1).

lee vortex takes on a more cork-screw form whereas winds parallel to the street are least interfered and generate channelling. In addition, variation in the building height modify these generalized patterns. As an example, buildings taller than the general roof level enhance the lee eddy of the lower buildings upwind (Oke, 1987; Gousseau et al., 2015). Due to its very complex nature, it is extremely difficult to find a single parameter to generalize the flow inside street canyons.

Analogous to buildings, vehicles modify the flow and produce vehicle-induced turbulence (VIT) (e.g. Kim et al., 2016; Thaker and Gokhale, 2016). The impact of VIT on the wind field at surface can be important especially if the wind velocity is low. However, this is out of scope of this study. In addition, apart from aerodynamic impacts of the urban obstacles on the flow, heterogeneous heating of walls and roofs and well as heat fluxes from buildings and vegetation modify the flow and generates turbulence, but the impact is found notably small compared to the aerodynamic effect of buildings except in very low wind conditions (Xie et al., 2005, 2007; Cai, 2012). Therefore, it is neglected here.

2.2.3 Aerodynamic impact of trees

In addition to buildings, trees are important roughness elements over an urban surface. Tree planting has many preferential impacts on an urban environment, for example, by increasing thermal comfort by providing shade, reducing noise problems and increasing biodiversity and aesthetics. Trees also modify the air flow, but due to their porous and flexible form, the effect is different from solid and inflexible buildings.

The impact of trees is double-edged. Firstly, air flowing over a vegetated surface generates aerodynamic drag on the foliage, which decelerates the flow within the canopy and its surroundings. Secondly, this deceleration generates turbulence in the following way. An inflection point (i.e. a change of the sign of the curvature of a curve) is formed in the vertical profile of the mean horizontal velocity as the flow is decelerated by the canopy top (Figure 4). The inflection point creates dynamic instabilities and can lead to formation of Kelvin-Helmholtz waves near the canopy top. As these waves break, further instabilities are introduced as the developing turbulence structure adapts a component in the direction of the main flow. Finally, large three dimensional turbulence structures are created (Raupach et al., 1996). Wind shear can generate turbulence dynamically even if the air is statically stable (Stull, 1988). On the other hand, dissipation rates are large in the canopy due to the fine-scale shear layers around the foliage and turbulence transfers momentum from the mean large scale flow to the smaller scales, which reduces shear and production of turbulence (Finnigan, 2000).

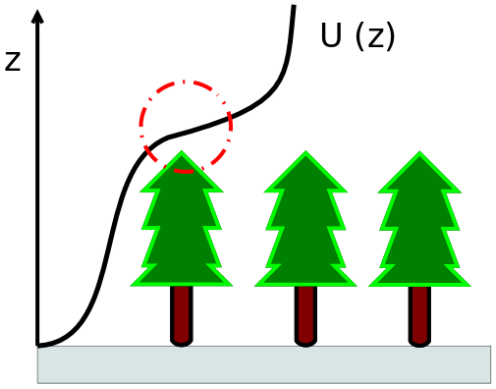

Figure 4: An idealized vertical profile of the mean horizontal wind speed $U(z)$ inside and above a plant canopy. The inflection point in the wind profile is marked with a red dash-dot circle.

Inside urban street canyons, the presence of street trees has mostly been found to reduce the wind speeds, especially on wide streets parallel to the mean wind, but also to accelerate the flow in some areas, similar to the acceleration of flow by the corners of buildings (Keck et al., 2014; Salim et al., 2015). Additionally, trees have been found to alter the vortex structures and to reduce the fluid mass circulation inside a street canyon (Gromke and Ruck, 2009; Gromke and Blocken, 2015; Salim et al., 2015). These blockage-related impacts disturb the vertical

transport of mass out of the canyon (Kikuchi et al., 2007; Mochida and Lun, 2008; Gromke and Ruck, 2009; Vos et al., 2013) and increase pollutant accumulation inside street canyons, especially near the leeward wall, compared to a treeless situation (Buccolieri et al., 2009; Gromke and Ruck, 2009; Gromke and Blocken, 2015). According to Buccolieri et al. (2009), the aspect ratio, as well as the wind direction and speed, are more crucial parameters affecting the deceleration of low than the tree stand density or the crown porosity. The decelerating effect of trees is most crucial in low wind conditions. Obviously, some areas can benefit from street trees but simultaneously hot-spots of pollutant concentrations can be developed in other places. Low vegetation near the source and vegetated walls have been found to increase pollutant deposition without blocking the wind and limiting dilution of clean air aloft (Pugh et al., 2012; Janhäll, 2015).

2.3 Dispersion and ventilation of pollutants

Dispersion and transport of pollutants in the PBL is controlled by atmospheric motions of various scales. In the along-wind direction, transport is dominated by the advection with the mean wind field, while in the across-wind and vertical directions turbulent eddies govern (Stull, 1988). The horizontal rate of transport and pollutant dilution are directly proportional to the speed of the mean wind field whereas atmospheric stability controls the vertical turbulent transport and the depth of the mixed layer sets an upper limit for mixing (Oke, 1987).

Transport and dispersion of pollutants over a city differs from that of its surroundings as buildings and surface heating enhance turbulence. Especially the mean horizontal wind has an important role in generating turbulence mechanically and therefore very calm wind conditions can lead to very poor air quality events. Direction of the mean wind field sets the path for pollutants and also pollutant input to the flow when the source is heterogeneous. But most importantly, the mean wind direction determines the formation of different wind patterns inside street canyons. For example, a canyon vortex (see Section 2.2.2) transports and accumulates pollutants emitted at the street level to the upwind side of the canyon (e.g. Baik and Kim, 2002). As an opposite, channelling occurs if the mean wind is parallel to a street and transport of pollutants by the horizontal advection is enhanced (Oke, 1987).

In an urban environment, vertical transport of pollutants is more desired than horizontal in order for pollutants to exit the pedestrian level where they are most harmful. The term "ventilation" has been used in previous studies to refer to city breathability i.e. the provision of cleaner air from above the UCL and vertical replacement of polluted air (Britter and Hanna, 2003; Buccolieri et al., 2010).

As the vertical transport is governed by turbulent eddies, ventilation is highly irregular. Typically, ventilation is stronger the smaller the aspect ratio of a street canyon is, i.e. the wider is the street compared to the building height. However, re-entrainment of pollutants from above to the street canyon has been found to decrease ventilation when the aspect ratio is decreased (Liu et al., 2011).

2.4 Numerical simulations

2.4.1 Large-eddy simulation

Computational fluid dynamics (CFD) is a study of flow of fluids by numerical simulations. It is applied both in fundamental research to understand, model and control physical mechanisms in flows, and in engineering to predict flow characteristics (Sagaut, 2006). The aim of CFD is to resolve the Navier-Stokes equations (see Equation 4). This can be achieved by using Direct Numerical Simulation (DNS). However, in the PBL, the turbulent flow has a large range of time and length scales. Computational costs of numerical simulations increase as Re^3 (Pope, 2000), where Re is the Reynolds number, and as $Re \sim 10^6 - 10^9$ in the PBL (Arya, 2001), solving all turbulent scales in the PBL is computationally very expensive and time consuming.

Large-eddy simulation (LES) is based on a filter separation of the turbulent motion into "large" scale eddies and sub-grid-scale (SGS) eddies. The large scales are directly numerically resolved by the three-dimensional prognostic Navier-Stokes equations (4) for momentum, temperature and humidity as well as for other relevant scalars. The impact of SGS eddies on the flow, instead, is modelled and added as an additional term to the tendency equations. Due to the non-linearity of the Navier-Stokes equation, different scales of flow are not resolved independently from each other as they are dynamically coupled (Sagaut, 2006). Additionally, the solution of LES depends, for instance, on the size of the computational grid relative to the phenomena being studied and the numerical method being applied. The applied filter width is selected so that the resolved large eddies account for most of the transport processes (Foken, 2008).

In a general filtering operation, the velocity field $\boldsymbol{u}(\boldsymbol{x}, t)$ is decomposed into a filtered, resolved-scale part $\widehat{\boldsymbol{u}}(\boldsymbol{x}, t)$ and a residual, SGS part $\boldsymbol{u}''(\boldsymbol{x}, t)$ (Pope, 2000):

$$\widehat{\boldsymbol{u}}(\boldsymbol{x}, t) = \int G(\boldsymbol{r}, \boldsymbol{x}) \boldsymbol{u}(\boldsymbol{x} - \boldsymbol{r}, t) d\boldsymbol{r}, \tag{6}$$

where G is the filter operator and $\boldsymbol{r}$ is the filter width vector. The SGS field is then defined by

$$\boldsymbol{u}''(\boldsymbol{x}, t) = \boldsymbol{u}(\boldsymbol{x}, t) - \widehat{\boldsymbol{u}}(\boldsymbol{x}, t), \tag{7}$$

which differs from the Reynolds decomposition (Equation 1) since in general

$$\overline{\boldsymbol{u}''}(\boldsymbol{x}, t) \neq 0 \tag{8}$$

To this day, most of the urban wind field studies have applied the Reynolds-Averaged Navier-Stokes (RANS) approach in which the Navier-Stokes equations are solved for the time-averaged quantity $\overline{\boldsymbol{s}}(\boldsymbol{x}, t)$ only. Furthermore, most of the RANS models are based on the linear eddy viscosity assumption and thus the method is less accurate if turbulent mixing is significant (Yazid et al., 2014). LES, on the other hand, resolves the instantaneous turbulence structures and not only the mean flow field averaged over the entire turbulence spectrum. This is important in order to investigate turbulent variations of flow which creates gustiness, modifies concentration fields and can enhance removal of pollutants from street canyons (Letzel et al., 2008). In addition, the mean flow around obstacles is calculated more accurately when applying LES (Gousseau et al., 2015; Keck et al., 2014; Tominaga and Stathopoulos, 2011). LES has been proved to compare well against measurements especially under near-neutral boundary conditions (e.g. Giometto et al., 2016). DNS is the most accurate approach but it is limited to flows with a small Reynolds number ($Re \sim 10^6 - 10^9$ in PBL) and a low number of scales due to high computational costs. As regards weaknesses, LES as well has high computational costs.

2.4.2 Urban air quality modelling

A large number of models with differing approaches and complexities have been developed over the years in order to study the dispersion of pollutants and the local air quality over urban surfaces (see e.g. Vardoulakis et al., 2003 and Tominaga and Stathopoulos, 2013 for reviews). Scientific understanding has improved in recent decades and the focus has turned to the street level where the largest concentration levels as well as highest number of people being exposed to are located. Mathematical and physical dispersion models are needed for regulatory purposes as well as for optimising the air quality monitoring, but also to study the impact of urban planning and future emission scenarios on air quality (Vardoulakis et al., 2003).

The most common dispersion models are Gaussian models which are based on parametrizing a pollutant plume from a line or a point source as a Gaussian distribution under steady-state conditions. The distribution of the plume is mainly determined by the atmospheric stratification and the wind velocity. Gaussian plume models are typically simple to use and modify to include more complicated phenomena, such as pollutant deposition (Tominaga and Stathopoulos,

2013). They are best suited for mesoscale modelling of pollutant concentrations at a distance of 100 m up to a few tens of kilometres from the source (Holmes and Morawska, 2006). Gaussian models have also been used over a complex terrain of a limited size but in addition to the closeness of sources, the models often fail to represent the plume behaviour in the turbulent flow accurately enough (Holmes and Morawska, 2006; Tominaga and Stathopoulos, 2013) likely because the surface parametrizations are often horizontally averaged and lack accuracy (Giometto et al., 2016).

Operational street pollution models are specifically designed semi-empirical parametric tools to provide time series of pollutant concentrations within a simplified street canyon layout. These models can be combined of models of different types, such as of a Gaussian plume model and a box model in order to take into account dispersion at several scales. Operational street pollution models are based on empirical assumptions and parameters, which reduces the amount of input data and the computational resources needed. Yet, recalibrations are required in new locations (Vardoulakis et al., 2003).

CFD dispersion models (see Section 2.4.1) can produce the entire flow and concentration fields with detailed information even over a very complex surface. Further advantages are, for instance, flexibility, adjustable grid spacing and advanced turbulence treatment (Holmes and Morawska, 2006). CFD dispersion models use either the Lagrangian or the Eulerian or their hybrid approach. In the Lagrangian approach, turbulent transport and dispersion are assessed by following the trajectories of finite elements or air parcels that are transported by the air flow. The Lagrangian approach is more suitable when the wind field is turbulent. The Eulerian models, instead, simulate concentrations of scalars in a fixed space and they are most applicable for studying long-range transport with chemistry included. The hybrid approach combines the two by applying the Lagrangian approach in the sub-grid scale and the Eulerian at the resolved scale (Li et al., 2006). Despite all advantages, CFD models are still currently too expensive for operational use and therefore they are especially applicable in scientific research (Blocken, 2015).

In addition to computational dispersion modelling, reduced-scale wind tunnel or water-tank simulations have been shown to be useful in studying pollutant dispersion, and especially in developing and validating models. They are based on the similarity principle, i.e. the original full-scale conditions are assumed to be reproducible from a study of a reduced scale. However, reduced-scale models are relatively difficult and expensive to set up and scaling can be problematic (Vardoulakis et al., 2003).

The right model to be utilized is chosen based on the scale of the studied phe-

nomenon and the capacities, assumptions and limitations of each model. Apart from selecting an appropriate model, conducting a model validation study and applying correct boundary conditions is important.

3 Applied numerical models

3.1 Parallelized Large-Eddy Simulation Model PALM

This study applies the Parallelized Large-Eddy Simulation Model (PALM) version 4.0 for atmospheric and oceanic flows (Maronga et al., 2015). It has been developed at the Institute of Meteorology and Climatology (IMUK) at Leibniz Universität Hannover, Germany, and the source code is free for scientific application. PALM has been applied in various types of boundary layer studies, for example to study the convective boundary layer over a heterogeneous surface (e.g. Hellsten et al., 2015), the impact of a plant canopy on the flow (e.g. Kanani-Sühring and Raasch, 2015) and the stable boundary layer (Beare et al., 2006). Furthermore, the model has been applied to study the urban boundary layer not only over idealized street canyons and buildings (e.g. Yaghoobian et al., 2014) but also over real urban surfaces (Letzel et al., 2012; Kanda et al., 2013; Keck et al., 2014). The performance of PALM over an urban-like surface has been validated against wind tunnel measurements, previous LES studies and observations (Letzel et al., 2008; Kanda et al., 2013; Razak et al., 2013; Park et al., 2015b).

PALM is based on solving the Navier-Stokes equations (4) for fluid properties assuming a non-hydrostatic and incompressible flow. The separation of the flow into the resolved scale ($\widehat{x}$) and the SGS scale (x'') is done according to Equations 6 and 7 over a grid volume on a Cartesian grid. In addition, Boussinesq approximation is applied, which states that the variation of the air density is only important in the buoyancy (gravity) term. Thus in Equation 4, ρ is replaced by the constant density ρ_0, except in the buoyancy term, and the gravitational acceleration g is written $-g(\widehat{\theta}-\langle\theta\rangle)/\langle\theta\rangle$ where $\langle\theta\rangle$ is the horizontal domain average of the potential temperature θ. In this study, we apply the dry version of PALM whereupon humidity is omitted. Finally, the prognostic equations for momentum (9), heat (10) and any scalar (11) are written

$$\begin{aligned}\frac{\partial\widehat{u}_i}{\partial t} = &-\frac{\partial\widehat{u}_i\widehat{u}_j}{\partial x_j} - \epsilon_{ijk}f_j\widehat{u}_k + \epsilon_{i3j}f_3\widehat{u}_{g,j} - \frac{1}{\rho_0}\frac{\partial\widehat{\pi}^*}{\partial x_i} \\ &+g\frac{\widehat{\theta}-\langle\theta\rangle}{\langle\theta\rangle}\delta_{i3} - \frac{\partial}{\partial x_j}\left(\overline{u_i''u_j''} - \frac{2}{3}e\delta_{ij}\right)\end{aligned} \tag{9}$$

$$\frac{\partial \widehat{\theta}}{\partial t} = -\frac{\partial \widehat{u}_j \widehat{\theta}}{\partial x_j} - \frac{\partial}{\partial x_j}\left(\overline{u_j'' \theta''}\right) \tag{10}$$

$$\frac{\partial \widehat{s}}{\partial t} = -\frac{\partial \widehat{u}_j \widehat{s}}{\partial x_j} - \frac{\partial}{\partial x_j}\left(\overline{u_j'' s''}\right) + \Psi_s. \tag{11}$$

Variable symbols are as in Equation 4 and the overlined products of the SGS terms are the SGS flux terms. Moreover, u_g is the geostrophic wind, $\pi^* = p^* + {}^2/_3\rho_0 e$ is the modified perturbation pressure where p^* is the perturbation pressure, $e = {}^1/_2\overline{u_i'' u_i''}$ is the SGS turbulent kinetic energy, s is any passive scalar (e.g. CO_2 concentration) and Ψ_s is the scalar source/sink term.

The SGS flux terms are produced as new unknowns as a result of the filtering process (Equations 6 and 7). They represent the impact of SGS on the resolved scales. However, they cannot be resolved explicitly which makes the choice of turbulence closure scheme very important. In the model, they are parametrized applying a 1.5-order sub-grid closure scheme based on Deardorff (1980). The parametrization assumes that the strength of the SGS fluxes is proportional to the local gradients of the mean quantities, e.g.

$$\overline{u_i'' u_j''} - \frac{2}{3} e \delta_{ij} = -K_m \left(\frac{\partial \widehat{u}_i}{\partial x_j} + \frac{\partial \widehat{u}_j}{\partial x_i}\right), \tag{12}$$

where the local SGS eddy diffusivity for momentum $K_m \propto \sqrt{e}$. Finally, the impact of the SGS motions on the large scale eddies is drawn by solving the prognostic equation for the SGS-TKE, as follows:

$$\frac{\partial \widehat{e}}{\partial t} = -\widehat{u}_j \frac{\partial \widehat{e}}{\partial x_j} - \left(\overline{u_i'' u_j''}\right) \frac{\partial \widehat{u}_i}{\partial x_j} + \frac{g}{\theta_0} \overline{u_3'' \theta''} - \frac{\partial}{\partial x_j}\left[u_j''\left(\widehat{e} + \frac{p''}{\rho_0}\right)\right] - \epsilon. \tag{13}$$

Here the last two terms, the pressure term and the SGS dissipation rate ϵ within a grid volume are parametrized as

$$\left[u_j''\left(e + \frac{p''}{\rho_0}\right)\right] = -2K_m \frac{\partial \widehat{e}}{\partial x_j} \quad \text{and} \tag{14}$$

$$\epsilon = \left(0.19 + 0.74 \frac{l}{\Delta}\right) \frac{\widehat{e}^{\frac{2}{3}}}{l}, \tag{15}$$

where l is the SGS length scale, which is proportional to height z and stratification, and $\Delta = \sqrt[3]{\Delta x \Delta y \Delta z}$ with Δx, Δy and Δz being the grid spacings in the x, y and z directions.

PALM is based on Fortran 95 programming language with several features of Fortran 2003. The model domain is spatially discretized using the Arakawa

staggered C-grid, in which all scalar variables are defined in the grid box centres whereas the velocity components are calculated on the box borders. The parallelization is realized by a two-dimensional domain decomposition method in which the three-dimensional domain is divided horizontally into equally-sized sub-domains along the x and y directions. Each sub-domain is assigned to one processor element which solves all model equations inside that sub-domain. Communication between sub-domains is realised using the Message Passing Interface (MPI). Computation of finite differences at the side boundaries of the sub-domains requires additional ghost layers that hold necessary data from its neighbouring sub-domains. We apply the 5th-order advection scheme of Wicker and Skamarock (Wicker and Skamarock, 2002), which requires three ghost layers. Moreover, stipulating incompressibility results in a Poisson equation (i.e. a partial differential equation) for the perturbation pressure term which is solved using an iterative multigrid scheme. Monin-Obukhov similarity theory (MOST) is applied at the bottom boundary between the surface and the first computational grid level normal to the surface with an assumption that MOST can be applied locally even over a heterogeneous surface (Maronga et al., 2015). Last of all, the time-integration is done by applying the 3rd-order Runge-Kutta approximation.

In this study, a full three-dimensional two-way self-nesting (Hellsten et al., 2016) is applied for the first time in LES studies applying PALM. In nesting, a "child" computational domain with a desired grid spacing and dimensions is defined inside the "parent" computational domain. PALM is run in parallel in both domains with respective computational set-ups. The models communicate in the following way. Firstly, the child domain model obtains the boundary conditions from the parent model. Secondly, the solution of the parent model is replaced by the restricted solution of the child model on each substep of the Runge-Kutta time-integration method. Nesting enables to have both a large computational domain and high enough resolution in the main area of interest without making the simulation computationally too expensive. This is important especially over urban surfaces where the flow characteristics are heterogeneous and detailed. Similar nesting method has already been applied in Nozu et al. (2008) to study the local urban flow field.

3.2 Canopy model

In PALM, the impact of vegetation on the flow and the exchange processes can be studied by means of an embedded canopy model (Maronga et al., 2015). In this study, only the aerodynamic effects are considered whereas the impact of heat fluxes or scalar sources and sinks are omitted. Vegetation is assumed to act

as a momentum sink due to the form and viscous drag forces. The decelerating impact of drag forces is included as an additional term in the tendency equations for momentum and SGS-TKE (see Equations 9 and 13), as follows:

$$\frac{\partial \widehat{u}_i}{\partial t}_{canopy} = -C_D \; PAD \sqrt{\widehat{u}_i^2}\widehat{u}_i \quad \text{and} \tag{16}$$

$$\frac{\partial \widehat{e}_i}{\partial t}_{canopy} = -2C_D \; PAD \sqrt{\widehat{u}_i^2}\widehat{e}, \tag{17}$$

where C_D is the aerodynamic drag coefficient and *PAD* is the plant area density ($\mathrm{m}^2\,\mathrm{m}^{-3}$). Typically, the aerodynamic impact of trees in urban areas is either neglected entirely or parametrized and taken into account in the definition of the surface roughness length (z_0) (Salim et al., 2015). However, Amorim et al. (2013) found the model performance to increase when trees were explicitly included as porous obstacles to the model simulation using an urban vegetation canopy model.

The embedded canopy model has mainly been developed for simple simulation set-ups with homogeneous plant canopies (e.g. the most recent study by Kanani-Sühring and Raasch, 2015). However, in this study the canopy layer over the computational domain is very heterogeneous. Firstly, the main area of interest is situated by the western border of the Central Park of Helsinki, which consists mostly of slightly managed woodland but also contains allotment gardens, vast field areas and large indoor sport centres. Secondly, two rows of street trees are planned to be planted along the city boulevard. Hence, the plant canopy model was revised by the author so that the height above sea level (ASL) of the plant canopy at each surface x, y-grid box is read into the model from a raster file (see Section 4.1).

In the model, the vertical profile of *PAD* and the decelerating impact of the canopy at each surface x,y-grid box is defined when the canopy height is above ground level at that point. The profile is given to the model by means of vertical gradients of *PAD* and levels at which the gradient changes. By the time of this study, one was able to input only one *PAD* profile for the whole computational domain. Therefore, the model was revised by the author so that the basic *PAD* profile is either vertically extended or packed if the canopy top at a surface x,y-grid box is over 4 m lower or higher than this profile. This approximation is decent because it is applied only outside of the planned city boulevard area.

3.3 Lagrangian stochastic particle model

PALM provides an embedded Lagrangian stochastic particle model (LPM) (Maronga et al., 2015; PALM, 2016) which was first applied in Steinfeld et al. (2008) to evaluate footprints (i.e. source areas) of particle concentration and flux. In LPM, Lagrangian particles are released inside assigned source volumes at selected moments in time, after which they are transported by the flow field inside the computational domain. Particle trajectories are defined from the locations of particles $\mathbf{X}_{\text{particle}}$ at each time step. At a new time $t + \Delta t$ the location is

$$\mathbf{X}_{\text{particle}}(\mathbf{X}_0, t + \Delta t) = \mathbf{X}_{\text{particle}}(\mathbf{X}_0, t) + \mathbf{V}_{\text{particle}}(\mathbf{X}_0, t)\Delta t, \tag{18}$$

where $\mathbf{X}_0$ is the spatial coordinate of the particle source point, t is the prior time and Δt is the time step used in the model, which can be equal to or smaller than the time step used in LES. In this study, particles are defined passive and massless, and rather comparable to air parcels. Hence, the effects of Stoke's drag and gravitational settling are insignificant, and the particle velocity $\mathbf{V}_{\text{particle}}$ can be defined

$$\mathbf{V}_{\text{particle}} = \mathbf{V}_{\text{resolved}} + \mathbf{V}_{\text{SGS}}, \tag{19}$$

where $\mathbf{V}_{\text{resolved}}$ is the resolved-scale part obtained by a tri-linear interpolation from the velocity field and $\mathbf{V}_{\text{SGS}}$ is the sub-grid-scale part resolved from the modified Langevin equation by Weil et al. (2004). This formulation assumes isotropic Gaussian turbulence and stochastic nature of SGS particle dispersion. Motion of massless particles can be considered similar to that of gaseous substances whereas for aerosols different physical and chemical processes should additionally be considered.

For this study, the LPM model, as well, was revised by the author to take into account the horizontal heterogeneity and the relative strengths of particle sources. The horizontal locations of the source areas are read into the model from a raster file (see Section 4.1) with a different integer value above zero for each different source group and a zero value for surface grid boxes without sources. All particles are released at a selected height with a constant particle release rate Q ($\#\ \mathrm{s}^{-1}\,\mathrm{m}^{-2}$). In order to consider different strengths of each source area, each particle group i inside the source area can be given a weight factor w_i and then the weighted particle concentration pc_{weight} in each grid box is calculated as

$$pc_{weight} = \sum^{N_i} w_i pc_i, \tag{20}$$

where $i \in \mathbb{Z}$ and pc_i is the particle concentration of each group i inside a grid box.

Weighting method is applied since the particle release rate must be high enough to represent a continuous source but small enough to limit the computational expenses.

4 Computational application

The simulations are made over a real urban surface, and thus the computational domain has several requirements to meet. Firstly, the domain size has to be large enough to capture all relevant turbulent scales, to minimize the uncertainties related to the boundary conditions and to vertically include the whole PBL. Secondly the grid spacing has to be small enough in order to explicitly resolve turbulence scales that contain most of the energy. In this study, the simulations are performed over a domain of 4096 m × 2048 m × 384 m (parent domain) in x-, y- and z-directions (Figure 5). Inside, a child domain of 2048 m × 1024 m × 96 m or 1536 m × 1536 m × 96 m, depending on the applied meteorological conditions, is defined. Within the child domain, a computational grid spacing of 1.0 m is applied in all directions whereas in the parent domain the grid spacing is 2.0 m.

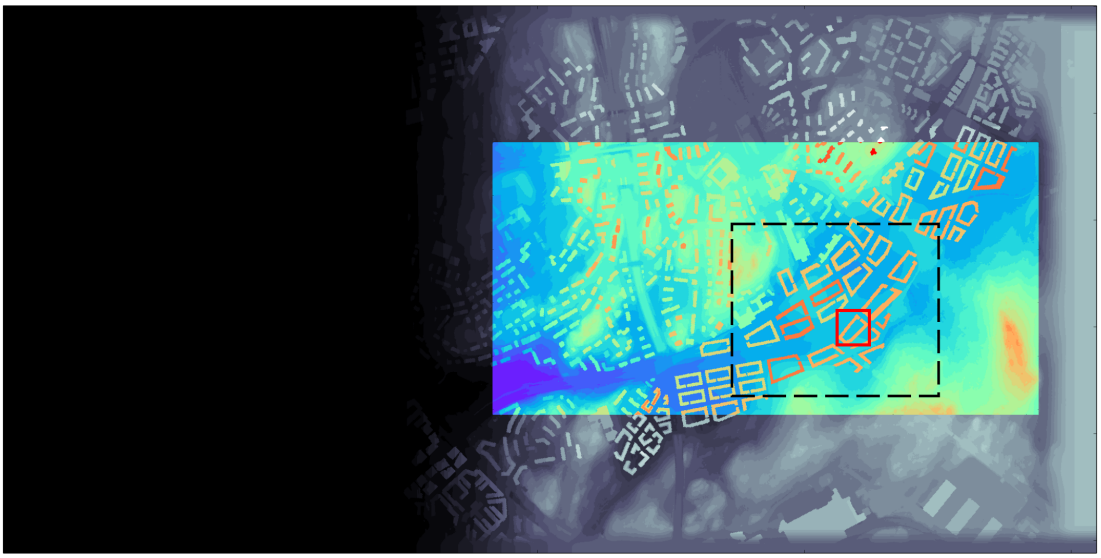

Figure 5: The computational domain with southwestern wind direction (WD = 225 °) and the city block design $\mathrm{V_{par}}$. The domain is separated into a child domain (rainbow shades) and a parent domain (grey shades), where the black shade stands for the topography elevation of $Z = 0$ m. The areas for collecting data output are marked with rectangles: the small domain with a solid red and the large domain with a black dashed line.

4.1 Urban surface data

The information on the surface elevation and cover is fed to the model as two-dimensional ASCII-formatted raster files. In the topography data each x,y -pixel in the raster file has a value for the elevation of topography Z(m) at that pixel. The topography data includes solid, impermeable and fixed flow obstacles which have a volume of at least one grid box, i.e. buildings and landform but not vehicles. No overhanging structures are accepted. Correspondingly, both the canopy model (see Section 3.2) and LPM (see Section 3.3) require separate raster files: for the canopy top height and for the horizontal locations of the particle sources inside the computational domain, respectively.

Information on the surface landform is drawn from the archive of the National Land Survey of Finland in ready-to-use format in raster tiles of 6 km $\times$ 6 km with a grid resolution of 2.0 m. The mean forest height is drawn from the archive of the Natural Resources Institute of Finland (Luke) similarly in ready-to-use format in a raster tile of 48 km $\times$ 96 km with a grid resolution of 20 m. All the rest including the existing and the planned buildings, the modified street network, the modified landform and the street trees to be planted is provided by the City Planning Department. This information, however, is provided in a sparsely meshed three-dimensional data format which requires further data manipulation.

The data from the City Planning Department is manipulated by the author in a following way. First this 3D-data are cut piece-by-piece into meshes with a smaller grid spacing using an open-source parametric 3D CAD modeller FreeCAD. Next the x-, y- and z-coordinates of each point in the tightly gridded meshes are saved into csv-formatted files using an open-source data analysis and visualization application ParaView. After that the building information in the csv-formatted files is saved over an empty ($Z = 0$ m) raster file by collecting the points in the mesh file to the representative pixel depending on the horizontal location and by giving the pixel the maximum Z value of these points. In order to fill unintentional holes inside buildings and to smooth building corners that could cause computational instability, median and minimum filters are applied separately for each raster file.

All topography information is superimposed on a single raster map file which is then pivoted according to the prevailing geostrophic wind in each simulation. Over the whole computational domain, Z is given in a vertical resolution of 2 m. A topography-free zone of around 1.4 km starting from the inflow boundary has to be set since a turbulence recycling method is used in the simulations (see Section 4.2). In addition, buffer regions of 20 m and 80 m where Z is smoothed towards values of 20 m and 35 m are added by the lateral boundaries and the

outflow region, respectively, in order to avoid computational instabilities and to satisfy the periodic boundary conditions.

4.1.1 Alternatives of city block design

In this comparative study, the numerical simulations using PALM are conducted applying four different city block design versions along the planned city boulevard. The initial state on Hämeenlinnanväylä without planned buildings is shown in Figure 6. In all versions, the average floor area is set to a constant value and the average number of floors is eight. The width of the city boulevard (i.e. the street) is 45 m and the total length is around 3.3 km. Including the walkways, the street canyon by the boulevard is around 58 m wide. Here, the alternative city block designs are given at the city planning level of detail, i.e. the amount of detail is minimal and, for example, balconies and bay windows are not considered. In addition, the impact of roof shape on the flow is not considered and thus all planned buildings have flat roofs. The design versions (V_{type} where type is either par, pen, perHV or J-J), are visualized in Figure 7 and their specific characteristics are listed below.

V_{par}: Building blocks by the boulevard are oriented so that the longest side is parallel to the boulevard and the building heights are fixed to 30 m.

V_{per}: Building blocks by the boulevard are oriented so that the longest side is perpendicular to the boulevard and the building heights are fixed to 30 m.

V_{perHV}: The orientation of the buildings by the boulevard is similar to the V_{per} but the height varies. The highest buildings are situated at the nodal points of the public transport, e.g. at the junction of Hämeenlinnanväylä and Metsäläntie (see Figure 7), whereas the lowest buildings as well as urban open spaces are situated between the nodal points.

V_{J-J}: A so-called "Jin-Jang" block model, in which buildings are similar to those in V_{par} but the base height is lower and narrower towers are set above the base. Thus the building shape and height are very irregular. According to the City Planning Department, this has been found to be the best compromise between minimizing the noise of the traffic inside the apartments and attaining a good air quality.

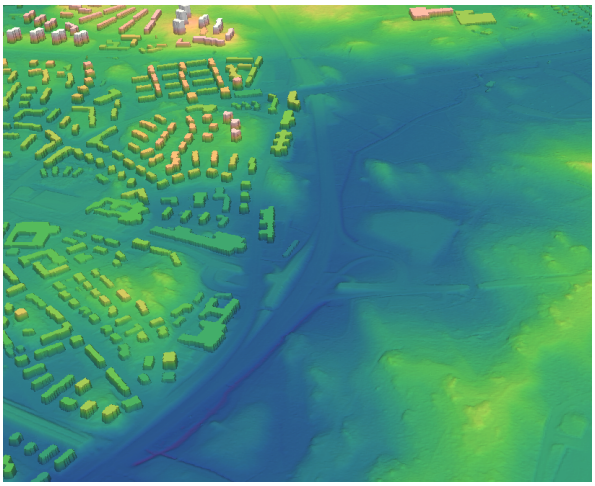

Figure 6: The initial state of the study site on Hämeenlinna in western Helsinki.

Figure 7: The city block design alternatives. From left to right: V_{par}, V_{per}, V_{perHV} and V_{J-J} (right). The boulevard (Hämeenlinnanväylä) is marked with a red line and the junction of Hämeenlinnanväylä and Metsäläntie with a black circle.

4.2 Boundary conditions

When nesting is applied in PALM, two runs are performed in parallel with different boundary conditions. The parent domain is given boundary conditions on its outer boundaries in the following way. At the bottom boundary, the no-slip condition with wall model (Maronga et al., 2015) applies for u and v, i.e. $u = v = w = 0$ m s^{-1}, whereas for θ the vertical gradient is set to zero. At the top boundary, $u = U_g$, i.e. the geostrophic wind speed, $v = 0$ and $w = 0$, and θ is extrapolated using the initial gradient of θ from a precursor run. For the child domain, the same conditions apply at the bottom boundary whereas a two-way nesting is applied at the top and horizontal boundaries. In the simulations, trees are considered only as porous material decelerating the flow, not as "boundaries".

A cyclic boundary condition is applied at the lateral boundaries whereas in

the streamwise direction the boundary condition is non-cyclic, i.e. the flow does not re-enter the domain after exiting at the outflow boundary. A time-dependent turbulent inflow is produced by a turbulence recycling method (Kataoka and Mizuno, 2002). This requires a precursor run over a flat surface with cyclic horizontal boundary conditions to create a turbulent field of a quasi-stationary state and mean profiles of the inflow field. The precursor run is carried out over a domain with the same vertical extent as the parent domain and $^1/_{16}$ in area, and random perturbations are added to the flow in the beginning to maintain turbulence. The PBL depth is set by initializing the precursor run with a θ-profile that has a strong gradient of $^{\partial\theta}/_{\partial z} = 30\,\mathrm{K\,km^{-1}}$ from the desired PBL height to the height of the outside computational domain (see Figure 8). This inversion prevents the PBL depth from increasing with time. The last time step of the precursor run is saved into a binary file and the main run is initialized by filling the domain cyclically with the precursor run data.

4.3 Meteorological conditions

The simulations are done for two different meteorological conditions by varying the wind speed U_g and direction WD and the atmospheric stratification (see Figure 8). The first set of runs are performed for a neutrally stratified PBL with a PBL height of 200 m and a geostrophic wind of $U_g = 10\,\mathrm{m\,s^{-1}}$ from the southwest ($WD = 225\,^\circ$) which is the most common wind direction in Helsinki (Pirinen et al., 2012). The surface heat flux is set to zero to maintain neutral stratification. This set-up is selected to represent the general conditions in Helsinki. Urban areas in Helsinki tend to be unstably stratified (e.g. Kurppa et al., 2015 and Karsisto et al., 2016), but applying a neutral stratification is a conservative choice as the turbulent removal of pollutants from street canyons is found to improve under unstable conditions (Cheng and Liu, 2011; Kikumoto et al., 2009). The second set of runs are performed for a (moderately) stable PBL with a PBL height of around 160 m and a geostrophic wind of $U_g = 8\,\mathrm{m\,s^{-1}}$ from the north-east ($WD = 90\,^\circ$) in order to study ventilation and dispersion in conditions that usually lead to the worst air quality events in Helsinki in winter if the Siberian high is prevailing. The atmospheric stratification and vertical wind profile applied are similar to the profiles in Basu and Porté-Agel (2006) and they are attained by performing the precursor run with these profiles and applying a surface heat exchange rate of $-0.006\,\mathrm{K\,m\,s^{-1}}$ to maintain the stable stratification. Simulating stably stratified PBL is a challenging task, since turbulent eddies are smaller and thus a relatively high resolution is needed in order to resolve most of the energy containing turbulence (Beare et al., 2006). In all runs, Coriolis force is applied

with $\phi = 60.16^\circ$ and the roughness length z_0 at surfaces is set to 0.05 m.

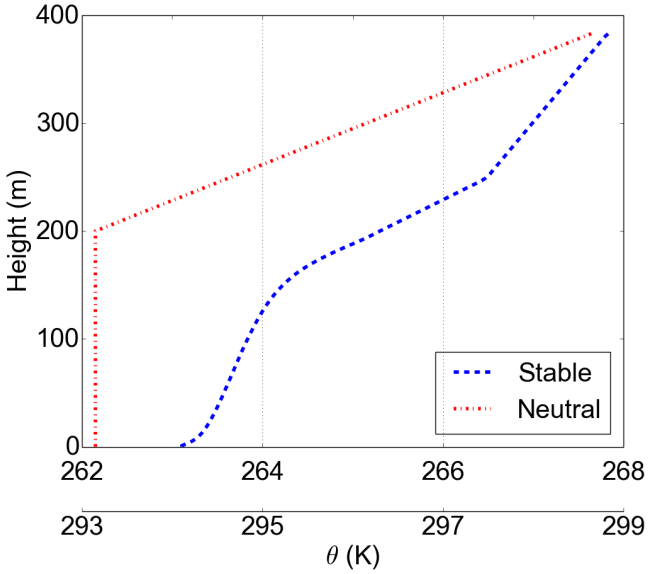

Figure 8: The vertical profile of potential temperature θ for the stable (blue dashed line, top x-axis) and the neutral (red dash-dot line, bottom x-axis) simulation.

4.4 Tree canopy

The trees to be planted along the city boulevard will be lime trees (*Tilia* × *vulgaris*) with the lowest branches at height of around 6.5 m. An experimental 5-year mean summertime value of the leaf area density $LAD = 5.3\,\mathrm{m^2\,m^{-3}}$ for *Tilia x vulgaris* trees in Viikki, Helsinki (Riikonen et al., 2016), is applied to construct the vertical profile of the plant area density (*PAD*). *LAD* considers only tree leaves whereas *PAD* takes the trunk and stems into account as well. The trees are assumed to have a circular cone shape, and hence the vertical profile of *PAD* is chosen to have a triangular shape with a maximum value at the height of the lowest branches and a surface value of $0.3\,\mathrm{m^2\,m^{-3}}$ (see Figure 9). Furthermore, when running simulations for a stably stratified PBL, the falling of leaves of deciduous trees before winter is simulated by decreasing the *PAD* values by 80 % following previous studies (e.g Muraoka et al., 2010; Groenendijk et al., 2011; Heiskanen et al., 2012 and Kimm and Ryu, 2015). When applying the canopy model in these simulations, the main interest is on the impact of the street trees on the boulevard. Thus, the *PAD* profiles of the surrounding trees outside of the boulevard area are defined similar to those of the street trees, but the profiles can be vertically extended or packed (see Section 3.2). In all simulations, $C_D = 0.2$ following previous LES studies over a tree canopy (e.g. Cassiani et al., 2008; Dupont and Brunet, 2008; Kanani-Sühring and Raasch, 2015).

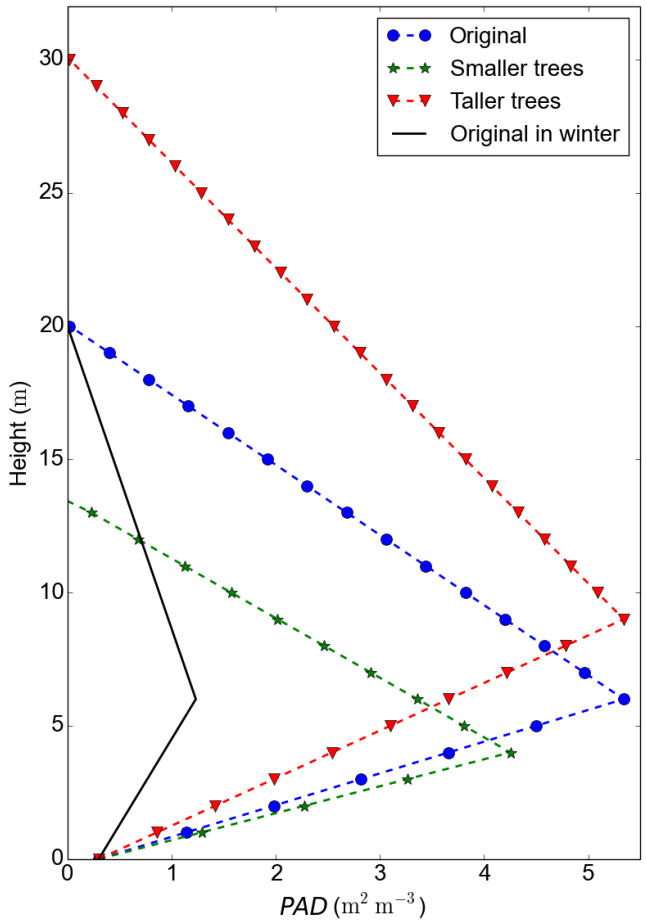

Figure 9: The vertical profile of *PAD* ($m^2\,m^{-3}$) for the street trees along the boulevard (blue dashed line with dots). Example profiles for trees that are smaller and taller than the boulevard trees are plotted in green (dashed line with stars) and red (dashed line with triangles), respectively. In addition, the winter time *PAD* profile for the street trees is given in black (solid line).

4.5 Particle model

In this study, the planned street network in the vicinity of the boulevard is defined as the source area (Figure 10) for inert and massless particles in the LPM (Section 3.3). Only the local traffic-related sources are taken into account similar to previous numerical ventilation studies (e.g. Liu et al. (2005)). This assumption is adequate enough for this study because ventilation, for instance, depends on the temporal variation of the concentration of a substance which is mainly governed by local sources and also because of the comparative nature of the study. The estimated traffic rates are provided by the City Planning Department and the impact of possible technological development on vehicle emissions is not considered.

Particles are released within each $1\,m \times 1\,m \times 1\,m$ surface grid box that is defined as a source at a constant rate of 0.25 $m^{-2}\,s^{-1}$. No particles are released below the street trees on the boulevard. The maximum age of particles is set to 800 s after which they exit the model. This is done in order to remove the particles stuck in the computational domain that increase the computational load. Particles are divided into three particle groups depending on the estimated traffic rate of each street inside the source area in year 2025. To take into account the

proportionally different traffic rates, the weighted particle concentration pc_{weight} (see Equation 20) is calculated by defining the weight factor for each particle group $i \in \{1, 2, 3\}$ as $w_i = 2^{i-1}$.

LPM is applied only inside the child domain. The particles released inside the child domain are restrained from entering the outside domain by setting an absorption condition at the vertical and top boundaries of the child domain. At ground, particles will be reflected. Detailed information about the specific boundary conditions in LPM can be found in Hellsten et al. (2015).

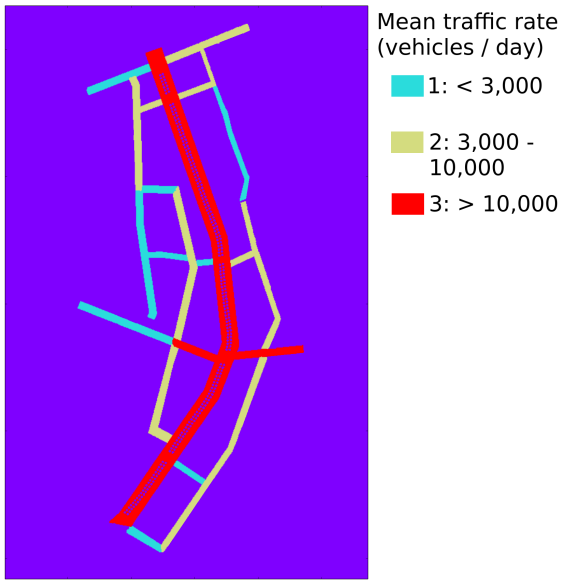

Figure 10: The planned boulevard street network in the block designs V_{par} and V_{J-J}, and the estimated traffic rates in year 2025. The streets are divided into three classes depending on the average traffic rates (see legends). Street surfaces below trees are omitted as source areas.

4.6 Simulations and data output

The simulations are performed in several parts. First, one precursor run per each meteorological condition is carried out over one hour and the final state is used to initialize the main runs. For the main runs, a time line of the simulation and the data output is depicted in Figure 11. The main run is carried out in batches of 55 minutes (batch 1) and 6 minutes (batch 2). The first batch stops at 55 minutes after which the second batch starts from the final state of the batch 1. The release of particles starts after 5 minutes from the start and is stopped at 56 minutes.

Data output is collected in three sequences and over two different domains of 0.5 km^2 and 0.02 km^2 (see Figure 5) after the system has reached a quasi-stationary state. The data output 1 with an interval of 5 s is collected over the large data output domain over a timespan of 40 minutes starting at 15 minutes. The collection of the data output 2 starts after 50 minutes with an interval equal to the integration time step of around 0.07 s and 0.15 s for neutral and stable runs, respectively. Due to the high logging frequency, the data output 2 is collected

only over the small output domain (see Figure 5). The data output 3 is collected over the large data output domain at an interval of 5 s during the last 5 minutes of the simulation after the particle release has been stopped. The vertical resolution is 1.0 m for all data output whereas the horizontal resolution is 1.0 m for the data output 2 and 2.0 m for the data outputs 1 and 3. The number of vertical levels is limited to 30 in order to limit the size of the output files.

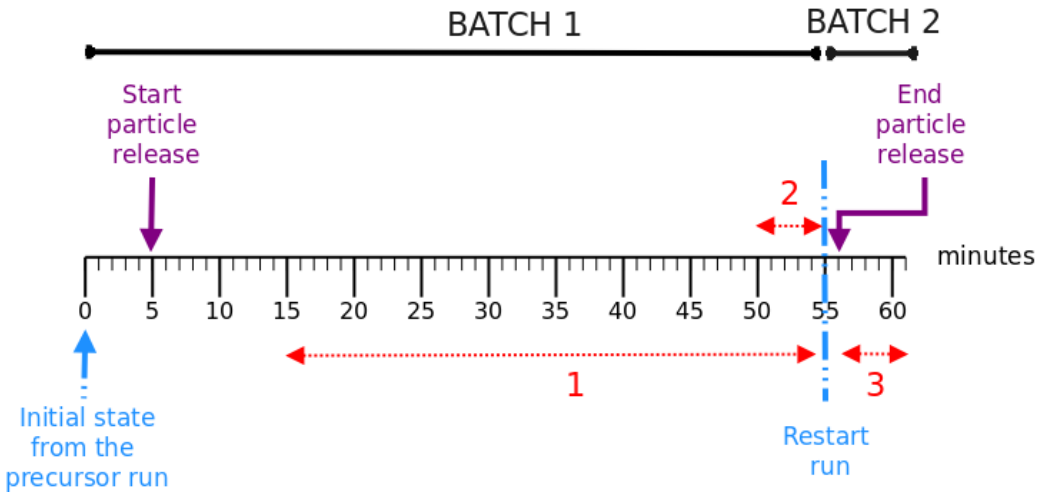

Figure 11: The simulation timeline for the main run. The time span of each data output (1, 2 and 3) is marked in red.

5 Results

From hereafter, particle number concentration $pc = pc_{weight}$ for the sake of simplicity. Furthermore, all heights are given in heights above ground level (AGL) unless otherwise specified. The junction of Hämeenlinnanväylä and Metsäläntie is referred to as the major junction and the surroundings refers to the surface area classified neither as a street canyon nor a courtyard, covering around 50 % of the large data output domain.

5.1 Particle number concentration

To give a general image of the distribution of particles inside each city block design version, *pc* are analysed. The 40-minute temporal mean and 90th percentile values of *pc* are studied at at two levels, $z = 4$ m and $z = 10$ m. Values are calculated from the data output 1 over the large data output domain for a layer between $z-1$ m and $z+1$ m in order to minimize random errors related to the vertical resolution of the topography data. The 90th percentile values (not shown) follow closely the mean values, and hence the mean values represent well the horizontal variability of *pc*.

The horizontal distributions of mean *pc* at $z = 4$ m are displayed in Figure 12. Values at $z = 10$ m are not shown. For the neutral runs (Figure 12a), the wind direction of the incoming flow is close to parallel to the southern part of the boulevard, whereas north of the major junction the mean wind has also a perpendicular component to the boulevard. The impact of wind direction relative to the boulevard can be seen in all concentration patterns: in the southern part of the boulevard concentrations are lower due to stronger transport of particles by the horizontal advection, and in the northern part particles are accumulated to the upwind side of the boulevard due to particle transport by a canyon vortex circulation (e.g. Baik and Kim, 2002). This also indicates that the formation of a canyon vortex is not completely inhibited by the presence of street trees. In the southern part of the boulevard, particle concentrations are slightly higher on the eastern side of the boulevard in all versions. Accumulation is more pronounced in V_{perHV} than V_{per} whereas the difference between V_{par} and V_{J-J} is smaller. Around the major junction, strong accumulation is observed in V_{perHV} inside the street canyon west of the junction where the building height decreases downwind. According to Nosek et al. (2016), stronger accumulation with a perpendicular wind can be explained by a typically weaker canyon vortex inside these kinds of step-down canyons. At the eastern entrance of the same canyons, similar hotspots are formed in V_{par} and V_{J-J}, but at the major junction concentrations are slightly higher in V_{J-J}. In the northern part, the hot-spots on the windward side of the boulevard are longer in V_{par} and V_{J-J} whereas in V_{per} and V_{perHV} ventilation from the cross streets breaks the accumulation patterns. Moreover, more corner vortices along the boulevard are formed in V_{per} and V_{perHV}, which can inhibit formation of a stable canyon vortex and pollutant accumulation (Vardoulakis et al., 2003). Yet, stronger hot-spots are formed in V_{per} than in V_{perHV}. This agrees with the findings of previous studies (Hoydysh and Dabberdt, 1988; Xiaomin et al., 2006; Nosek et al., 2016) showing that concentrations on the windward side are typically lower for a step-up canyon, as in V_{perHV}, than in a symmetrical canyon, as in V_{per}. In V_{J-J}, another hotspot is formed on the downwind side of the canyon. In general, *pc* values are of the same magnitude in V_{par} and V_{J-J}, indicating that aerodynamically rougher buildings in V_{J-J} do not notably improve the air quality near the pedestrian level. Over the cross streets the differences are not that distinct as over the boulevard. Generally, concentrations appear to be horizontally better mixed in V_{per} and V_{perHV} than in V_{par} and V_{J-J}. The courtyards are notably clean and the concentrations remain low throughout all simulations.

Figure 12b displays *pc* for the stable runs. Despite the lower *PAD* values of the street trees in the stable runs, *pc* at $z = 4$ m are around two-fold compared

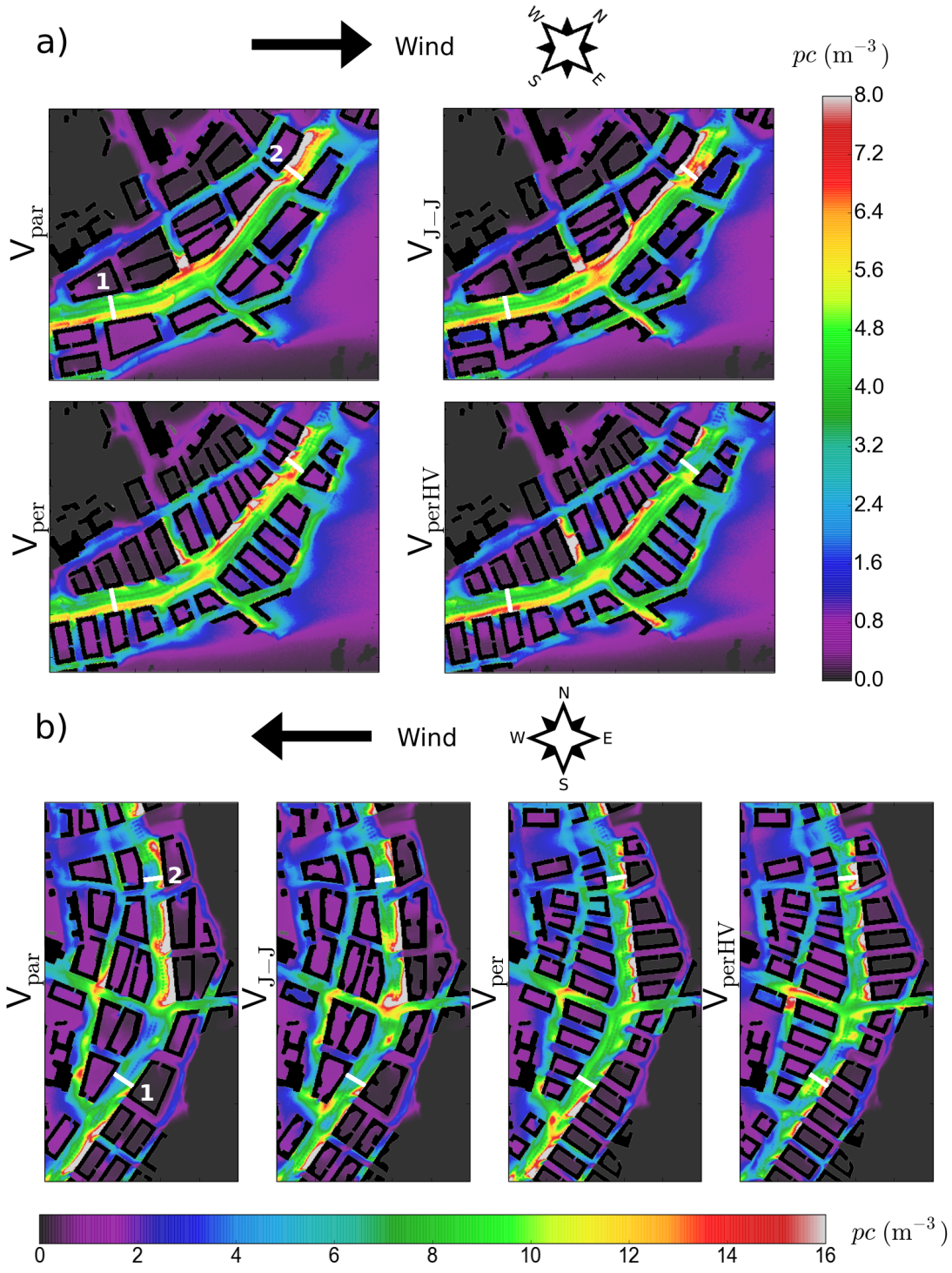

Figure 12: 40-minute mean particle concentration pc (m^{-3}) at $z = 4$ m for a) the neutral runs with $WD = 225$ ° and b) the stable runs with $WD = 90$ °. Notice the orientation of the mean wind and the different scales of pc in a) and b). Cross sections in Figure 13 are marked in white.

to the neutral runs, which shows the important role of atmospheric stratification in pollutant dispersion. As the wind direction is close to perpendicular to the boulevard, the cross streets provide fresh, unpolluted air from the east and the

mean concentrations along those streets are low. Furthermore, pollution patterns along the boulevard are strongly related to the location of the cross streets. As for the neutral runs, the hot-spots on the windward side of the boulevard in V_{per} and V_{perHV} are broken by ventilation from the cross streets. In V_{J-J}, *pc* values are slightly elevated on the downwind side of the higher towers of buildings compared to V_{par}. On the whole, hot-spots differ in the shape and size between all versions. For instance, in the southern part of the boulevard (top-right corner) the strongest and vastest hotspots are formed in V_{par} and V_{per} whereas the step-up type of the canyons in V_{perHV} reduces pollutant accumulation. On the contrary, around the major junction *pc* are a little higher inside V_{perHV} than in the symmetrical V_{per}, which can be explained by the step-down type of the canyon as the building height in V_{perHV} decreases westward from the upwind side of the boulevard. Yet, *pc* values north of the major junction are not distinctly higher in V_{perHV} than in V_{per} despite the step-down type of V_{perHV}. Similar to the neutral runs, *pc* values in V_{par} and V_{J-J} are of the same order of magnitude and the courtyards remain clean. Another notable feature is the accumulation of particles behind the upwind corners of buildings, especially on the boulevard. According to Gromke and Ruck (2009), this can explained by the presence of street trees that hinder the corner eddies and reduces ventilation locally.

Two vertical cross sections marked in Figure 12 are shown in Figure 13a and b for the neutral, and c and d for the stable runs. Cross section 1 is for the southern part and Cross section 2 for the northern part of the boulevard. The figure illustrates the vertical dispersion of *pc* and mean wind vectors inside the street canyon at two separate locations and thus the representativeness is limited. However, the figure visualises the dependence of *pc* on both urban morphology and meteorological conditions. Clean air can be seen to penetrate the canyon from above. However, street trees decelerate the flow and hinder the canyon vortex in the neutral runs due to a higher *PAD*. This explains, for instance, the accumulation of *pc* on both sides of the boulevard in V_{J-J} in Figure 12a and b. A uniform vortex is seen only in Cross sections 1 for the stable runs (Figure 12c), yet the location varies between versions. Vertical maxima of *pc* are seen at the maximum of the *PAD* profile at $z = 6.5$ m, i.e. at around $z = 15$ m above sea level in Figure 12.

Horizontal mean *pc* at $z = 4$ m and $z = 10$ m separately for the boulevard, the other street canyons, the courtyards and the surroundings are presented in Table 1. In almost all cases, the ranking of different design versions is similar at both levels. Above the boulevard, both the mean and 90th percentile values are lowest in V_{perHV} for both the neutral and stable runs whereas highest values are observed in V_{J-J} and V_{per} for the neutral and stable runs, respectively. Previous

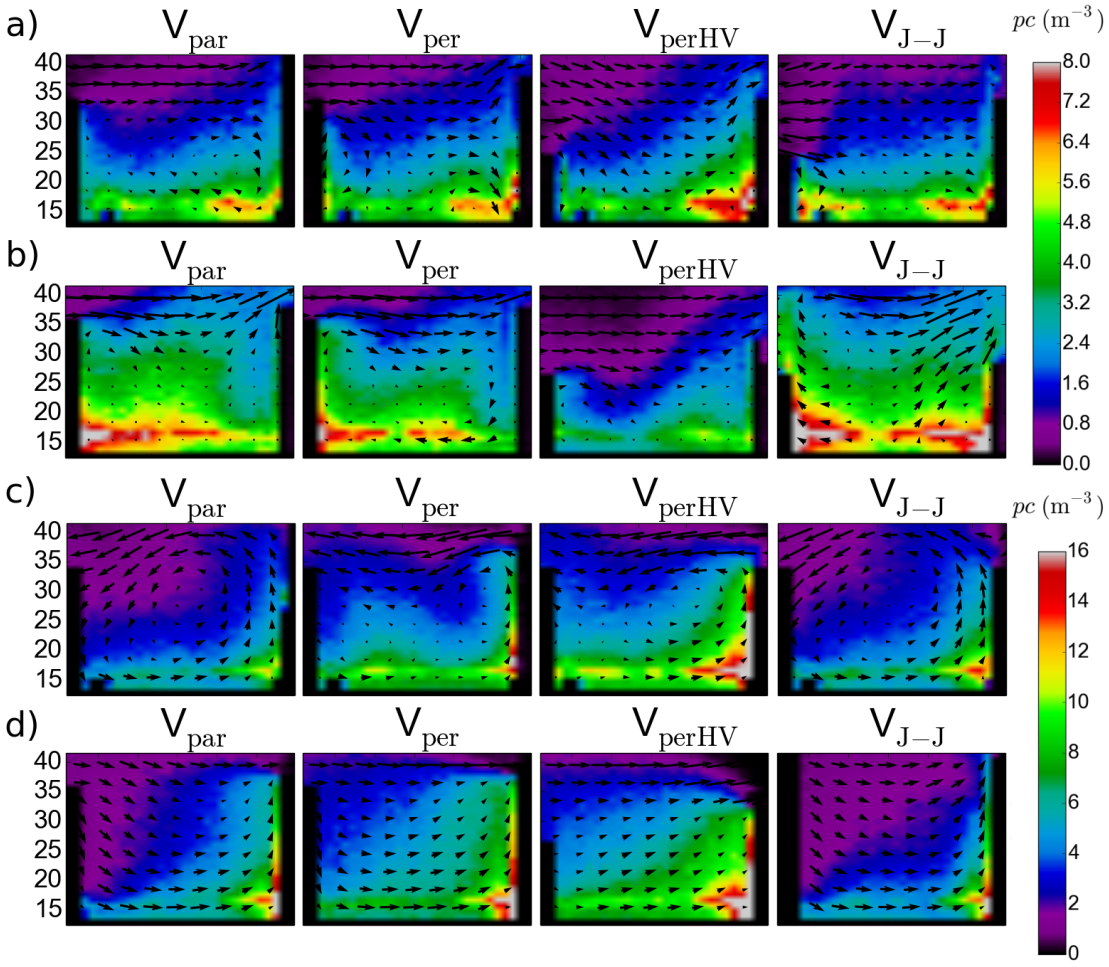

Figure 13: 40-minute mean particle concentration pc (m^{-3}) across the boulevard. Cross sections 1 and 2 (see Figure 12) are shown in a) and b) for the neutral runs and in c) and d) for the stable runs, respectively. Cross sections are viewed from the south. The height given on the left is height in metres above sea level. Additionally, wind vectors are plotted as arrows to display the mean flow field.

studies have shown that particle concentrations are typically lower in shorter street canyons (Dabberdt and Hoydysh, 1991; Ossanlis et al., 2007; Michioka et al., 2014), which agrees with the lowest values in $\mathrm{V_{per}}$ and $\mathrm{V_{perHV}}$, except for the stable runs. Inside the other street canyons, the ranking is more complex. As for the neutral runs, $\mathrm{V_{par}}$ performs best and $\mathrm{V_{per}}$ and $\mathrm{V_{perHV}}$ worst whereas for the stable runs, $\mathrm{V_{J-J}}$ performs best and $\mathrm{V_{par}}$ worst. Inside the courtyards, $\mathrm{V_{par}}$ has the lowest values in both meteorological conditions while the highest are observed in $\mathrm{V_{J-J}}$ and $\mathrm{V_{perHV}}$. Also in the surroundings, $\mathrm{V_{par}}$ performs constantly best whereas $\mathrm{V_{per}}$ has the highest values. In conclusion, the ranking of block design versions based on the mean and 90th percentile values of pc is different for different parts of the city boulevard and it is also strongly dependent on the meteorological conditions.

Table 1: 40-minute horizontal mean particle concentrations pc (m^{-3}) separately for the boulevard, the other street canyons, the courtyards and the surroundings at heights $z = 4$ and $z = 10$ m for all runs. 90th percentile values are given inside brackets. The best values are marked in blue and the worst in red.

Boulevard					
Run	z	V_{par}	V_{per}	V_{perHV}	V_{J-J}
Neutral, 225°	4 m	4.82 (8.61)	4.51 (8.23)	4.27 (7.98)	4.98 (8.97)
	10 m	2.81 (5.74)	2.69 (5.55)	2.39 (5.16)	2.84 (5.85)
Stable, 90°	4 m	8.51 (14.12)	8.83 (14.70)	7.63 (12.80)	8.37 (13.94)
	10 m	5.25 (9.54)	5.41 (9.97)	4.53 (8.46)	4.87 (9.04)
Other street canyons					
Run	z	V_{par}	V_{per}	V_{perHV}	V_{J-J}
Neutral, 225°	4 m	2.14 (4.00)	2.26 (4.19)	2.33 (4.33)	2.18 (4.08)
	10 m	1.28 (2.71)	1.41 (2.95)	1.38 (2.93)	1.28 (2.73)
Stable, 90°	4 m	4.67 (7.66)	4.58 (7.67)	4.50 (7.52)	4.25 (7.10)
	10 m	2.80 (5.14)	2.68 (5.08)	2.60 (4.97)	2.56 (4.76)
Courtyards					
Run	z	V_{par}	V_{per}	V_{perHV}	V_{J-J}
Neutral, 225°	4 m	0.56 (1.54)	0.58 (1.66)	0.64 (1.80)	0.74 (1.94)
	10 m	0.56 (1.54)	0.58 (1.64)	0.63 (1.79)	0.75 (1.95)
Stable, 90°	4 m	0.71 (1.80)	0.83 (1.86)	0.88 (2.01)	0.79 (1.91)
	10 m	0.72 (1.81)	0.81 (1.83)	0.87 (2.01)	0.78 (1.91)
Surroundings					
Run	z	V_{par}	V_{per}	V_{perHV}	V_{J-J}
Neutral, 225°	4 m	0.69 (1.62)	0.82 (1.87)	0.75 (1.75)	0.70 (1.66)
	10 m	0.62 (1.51)	0.74 (1.76)	0.67 (1.63)	0.63 (1.55)
Stable, 90°	4 m	1.09 (2.09)	1.20 (2.29)	1.12 (2.16)	1.09 (2.09)
	10 m	0.92 (1.86)	1.04 (2.06)	0.94 (1.89)	0.94 (1.87)

5.2 Ventilation

Ventilation refers to replacement of polluted air by fresh air. In this study, ventilation of street canyons and courtyards is assessed by calculating the vertical turbulent particle flux density (F_p, Section 5.2.1) and the particle dilution rate (D, Section 5.2.2). Various other measures have also been proposed and used in previous ventilation studies over urban surfaces, for instance the particle exchange rate (assumes horizontal homogeneity of pc, Liu et al., 2005), the velocity ratio (in e.g. Keck et al., 2014), the mean tracer age and age distribution (Lo and Ngan, 2015) and the exchange velocity (Bentham and Britter, 2003). However, the studies have been conducted over idealistic canyons. F_p was chosen to be applied in the analysis since it is a measure elaborate enough without making the analysis too complex over a very heterogeneous surface. Additionally, D is

regarded to give a physically reasonable estimate of the ventilation capacity of a street canyon or a courtyard.

5.2.1 Turbulent particle flux density

Vertical turbulent particle flux density F_p is calculated as the covariance between the vertical wind velocity and the particle number concentration (Stull, 1988), as follows:

$$F_p\left(x,y,z\right) = \overline{w'\left(t,x,y,z\right)\, pc'\left(t,x,y,z\right)}\ , \tag{21}$$

where $w'\left(t,x,y,z\right)$ and $pc'\left(t,x,y,z\right)$ are the instantaneous fluctuating vertical velocity and particle number concentration at point (x,y,z) at time t. Positive F_p indicates upward particle transport, i.e. ventilation, and negative downward particle transport, i.e. re-entrainment of pollutants from air above. Hence, the higher F_p, the higher ventilation. Previously, particle flux densities have been analysed in CFD studies over idealized street canyons (e.g. Baik and Kim, 2002; Walton and Cheng, 2002; Liu et al., 2004; Nosek et al., 2016). Turbulent flux densities have been shown to be responsible for pollutant removal from idealized street canyons (Li et al., 2009; Liu et al., 2015) whereas re-entrainment of pollutants from above into the street canyons and the courtyards is caused by advective flux densities (Baik and Kim, 2002). However, turbulence governs at roof level (e.g. Nosek et al., 2016), and thus only the turbulent flux density F_p is applied in the analysis.

In this study, F_p are calculated both from the high-frequency data output 2 over the small domain ($F_{p,HF}$) and the low-frequency data output 1 over the large domain ($F_{p,LF}$). The analysis height is chosen $z = 20$ m, which is the minimum roof height of all versions. Before calculating the covariances, linear de-trending is applied on both time series. As regards the low logging frequency of 0.2 Hz of the data output 1, a notable proportion of the total vertical turbulent flux density may be missed and thus the exact values of $F_{p,LF}$ should be treated with caution. On the other hand, representativeness of $F_{p,HF}$ calculated only over the small data output domain is rather limited. Therefore, $F_{p,HF}$ is compared to $F_{p,LF}$ over the same domain in order to show the applicability of $F_{p,LF}$ in this comparative study.

Figure 14 displays $F_{p,HF}$ for all versions for both the neutral (a) and stable (b) runs. Based on this figure, it is difficult to distinguish clear differences between the versions. Generally, $F_{p,HF}$ is largest above the boulevard and smallest inside the courtyards where $F_{p,HF}$ can be negative indicating downward particle transport. Inside the courtyards, $F_{p,HF}$ is larger in magnitude in the neutral runs than in the stable runs. According to Moonen et al. (2011), the vertical exchange above a

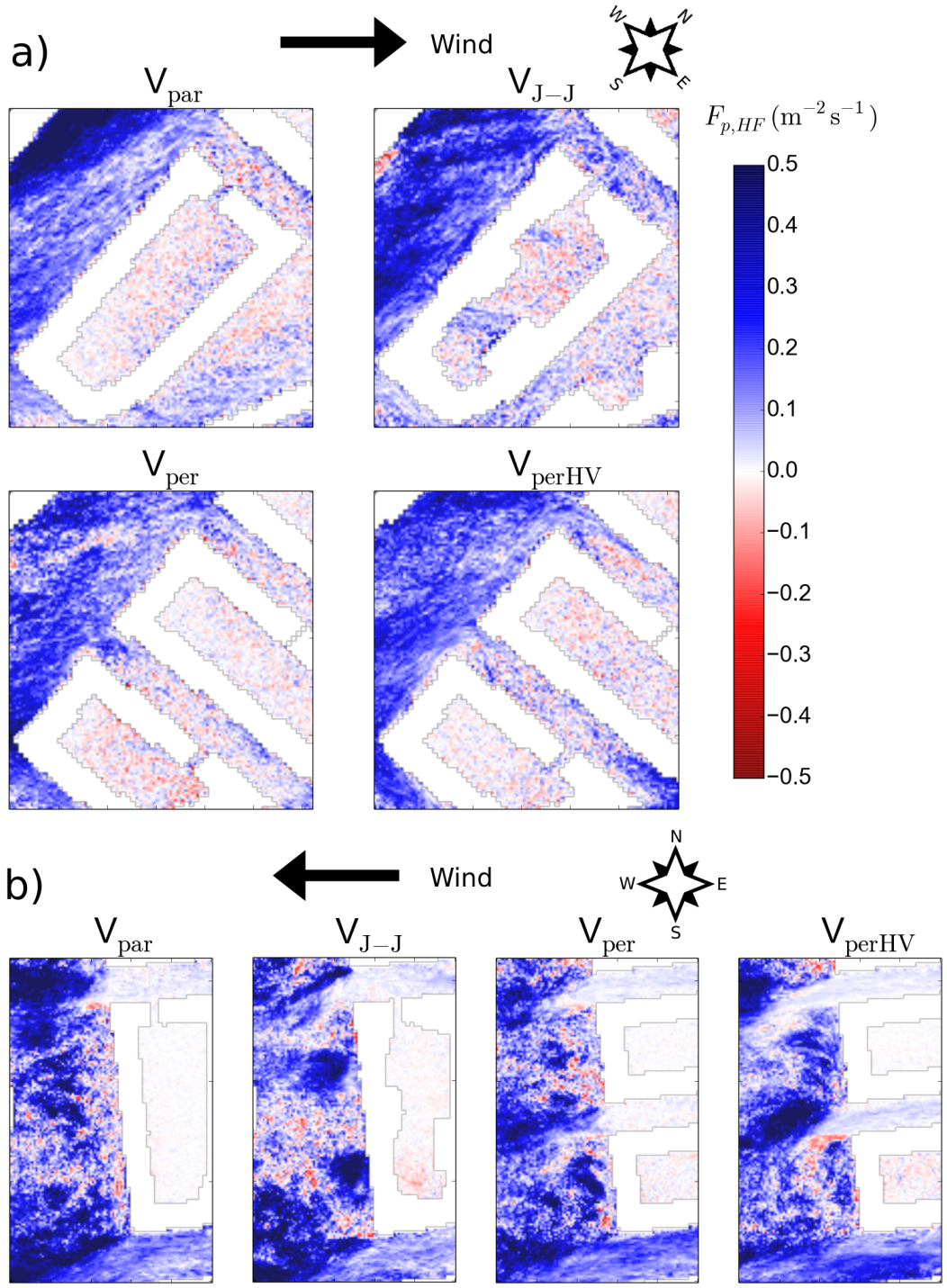

Figure 14: 40-minute mean high-frequency turbulent particle flux density $F_{p,HF}$ ($\mathrm{m^{-2}\,s^{-1}}$) at $z = 20$ m for a) the neutral runs with $WD = 225$ ° and b) the stable runs with $WD = 90$ °. The analysis area is marked in Figure 4 in red.

courtyard is lowest when the angle between the wind and the principal courtyard axis is around 90 °, which is the case in the stable runs. As for the stable runs, $F_{p,HF}$ is small above the cross streets where advective transport is likely to govern. Figure 14b also shows how particle exchange is weakened behind the upwind corners of buildings and the higher towers in $\mathrm{V_{J-J}}$ (seen as wider parts in

the building width), which can explain the particle accumulation seen in Figure 12b.

Table 2: Horizontal mean of the high-frequency turbulent particle flux density $F_{p,HF}$ ($\mathrm{m^{-2}\,s^{-1}}$) separately for the boulevard, the other street canyons and the courtyards at $z = 20$ m for all runs. Horizontal mean of the low-frequency turbulent particle flux density $F_{p,LF}$ over the same domain is given in brackets. The best values are marked in blue and the worst in red.

Boulevard				
Run	V_{par}	V_{per}	V_{perHV}	V_{J-J}
Neutral, 225°	0.193	0.162	0.169	0.213
	(0.233)	(0.238)	(0.292)	(0.247)
Stable, 90°	0.221	0.168	0.159	0.178
	(0.294)	(0.209)	(0.211)	(0.191)
Other street canyons				
Run	V_{par}	V_{per}	V_{perHV}	V_{J-J}
Neutral, 225°	0.085	0.078	0.247	0.117
	(0.054)	(0.056)	(0.138)	(0.102)
Stable, 90°	0.115	0.141	0.180	0.102
	(0.120)	(0.120)	(0.229)	(0.111)
Courtyards				
Run	V_{par}	V_{per}	V_{perHV}	V_{J-J}
Neutral, 225°	2.2×10^{-3}	-3.5×10^{-3}	1.1×10^{-3}	17.1×10^{-3}
	(-4.5×10^{-3})	(0.8×10^{-3})	(1.2×10^{-3})	(16.7×10^{-3})
Stable, 90°	-0.0×10^{-3}	-0.4×10^{-3}	-2.0×10^{-3}	-5.6×10^{-3}
	(0.5×10^{-3})	(-2.0×10^{-3})	(-4.3×10^{-3})	(-7.7×10^{-3})
Surroundings				
Run	V_{par}	V_{per}	V_{perHV}	V_{J-J}
Neutral, 225°	0.038	0.039	0.058	0.045
	(0.026)	(0.040)	(0.071)	(0.047)
Stable, 90°	0.043	0.041	0.045	0.037
	(0.085)	(0.059)	(0.057)	(0.074)

Horizontal mean values of $F_{p,HF}$ as well as $F_{p,LF}$ above the same small data output domain are given separately for the boulevard, the other street canyons, the courtyards and the surroundings in Table 2. Overall, $F_{p,HF}$ and $F_{p,LF}$ show rather similar ranking of the design versions except above the boulevard for the neutral runs and in the surrounding for the stable runs. A Student's one-sample t-test for the difference of the exact values of $F_{p,HF}$ and $F_{p,LF}$ shows that the difference is insignificant at 95 % confidence level ($p = 0.069$). $F_{p,HF}$ and $F_{p,LF}$ values agree better for the stable than for the neutral runs. This is most likely due to the longer time step of the stable runs which is nearly threefold to that for the neutral runs. If $F_{p,HF}$ for the neutral runs is calculated using only every other time step of the data output 2, the difference becomes even less significant

($p = 0.18$). Therefore $F_{p,LF}$ can be applied when comparing the different city block design versions instead of $F_{p,HF}$.

Figure 15 shows $F_{p,LF}$ for all versions for both the neutral (a) and stable (b) runs for the larger data output domain. For all runs, $F_{p,LF}$ appears to be on

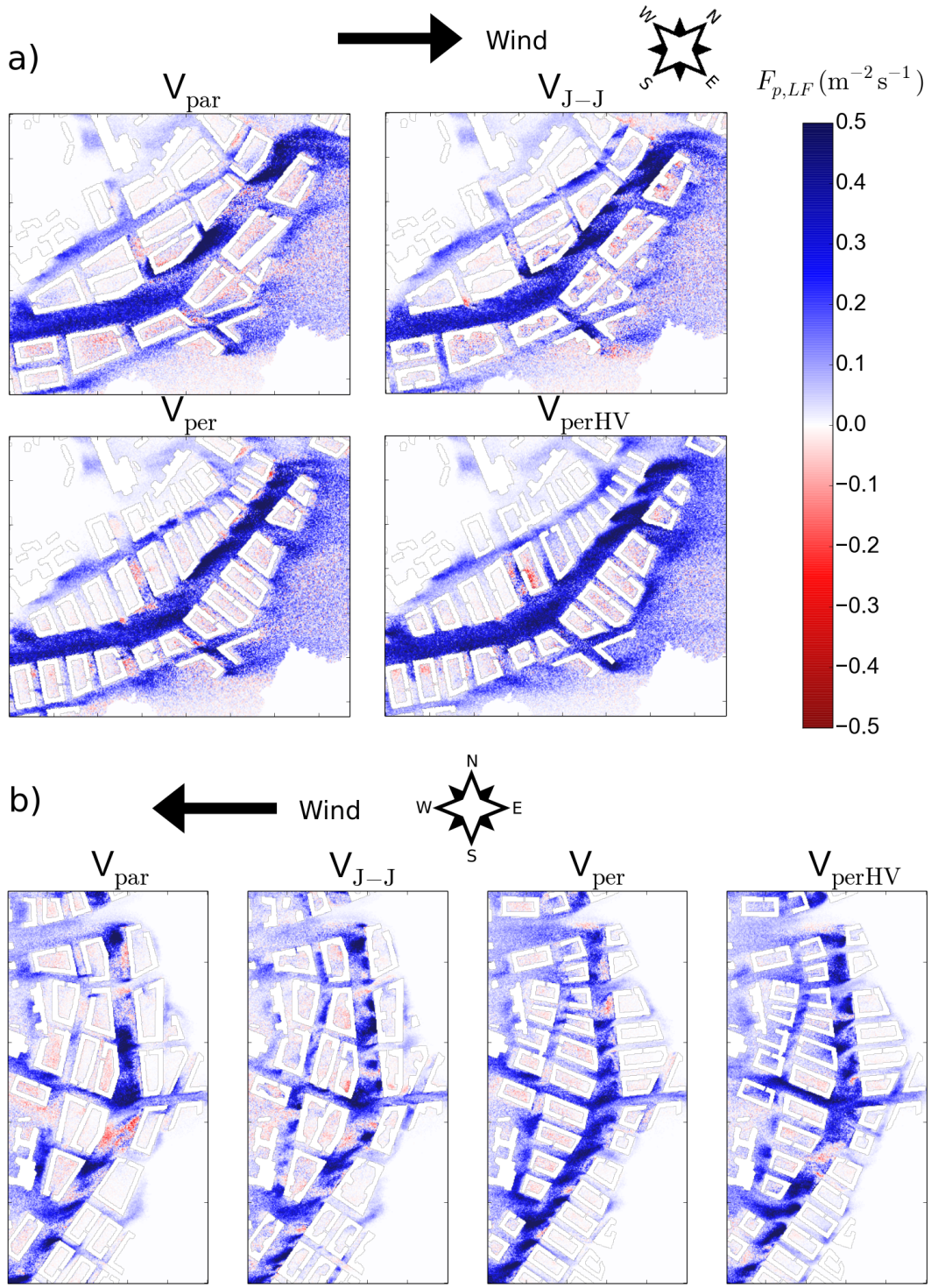

Figure 15: 40-minute mean low-frequency turbulent particle flux density $F_{p,LF}$ ($\mathrm{m^{-2}\,s^{-1}}$) at $z = 20$ m for a) the neutral runs with $WD = 225$ ° and b) the stable runs with $WD = 90$ °.

average positive in all versions indicating upward transport of particles and ventilation. This can be expected since the particle source is constantly maintaining *pc* at street level. In general, $F_{p,LF}$ is larger above the source i.e. above streets, while inside the courtyards the flux density is close to zero or even negative, which was also seen in Figure 14. Furthermore, $F_{p,LF}$ values are smaller for the stable than for the neutral runs, which is due to the weaker vertical mixing in stably stratified atmosphere (Tomas et al., 2016), resulting in higher concentrations near the surface (see Figure 12). For the neutral runs, flux density appears to be most positive along the boulevard in $\mathrm{V_{perHV}}$, whereas in the other versions, areas of negative flux density (re-entrainment) also appear along the boulevard. Similar to *pc*, building height variability appears favourable for $F_{p,LF}$ in this wind direction while building shape variability in $\mathrm{V_{J-J}}$ does not seem to have any notable impact. On the other hand, west of the major junction in $\mathrm{V_{perHV}}$, flux density is negative both above the street canyon and courtyard, which is linked to the step-down type of the canyon. As for the stable runs, flux density appears to be most positive in $\mathrm{V_{per}}$ and $\mathrm{V_{perHV}}$. In $\mathrm{V_{par}}$, there is a vast area of negative flux density south of the major junction. The same is seen in $\mathrm{V_{J-J}}$ but less pronounced. In $\mathrm{V_{J-J}}$, $F_{p,LF}$ decreases downwind of the higher towers of the buildings and in $\mathrm{V_{perHV}}$, $F_{p,LF}$ is slightly decreased downwind of the highest buildings along the boulevard where the canyon is of step-down type. Additionally, $F_{p,LF}$ generally decreases upwind of the junction of cross streets and the boulevard, as seen also in Figure 14b.

Horizontal mean values of $F_{p,LF}$ separately for the boulevard, the other street canyons, the courtyards and the surroundings are given in Table 3. Values correspond well to the visual analysis made based on Figure 15. Values are higher for the neutral runs, showing the dependence of turbulent transport on stability. For the neutral runs, $F_{p,LF}$ is largest above the boulevard, the other streets and the surroundings in $\mathrm{V_{perHV}}$ and above the courtyards in $\mathrm{V_{J-J}}$. $F_{p,LF}$ is smallest above all street canyons in $\mathrm{V_{par}}$, above the courtyards in $\mathrm{V_{per}}$ and in the surroundings in $\mathrm{V_{J-J}}$. As for the stable runs, $F_{p,LF}$ is highest above the boulevard and in the surroundings in $\mathrm{V_{per}}$, and above the other street canyons and courtyards in $\mathrm{V_{perHV}}$. $F_{p,LF}$ is smallest above the boulevard in $\mathrm{V_{J-J}}$, above the other street canyons and courtyards in $\mathrm{V_{par}}$ and in the surroundings in $\mathrm{V_{J-J}}$. Overall, $\mathrm{V_{perHV}}$ appears to perform best according to mean $F_{p,LF}$ values.

5.2.2 Particle dilution rate

The second measure to evaluate ventilation is the particle dilution rate D. The particle source at ground is switched off at 56 min of the simulation after which

Table 3: Horizontal mean of the low-frequency turbulent particle flux density $F_{p,LF}$ ($m^{-2}\,s^{-1}$) separately for the boulevard, the other street canyons, the courtyards and the surroundings $z = 20$ m for all runs. The best values are marked in blue and the worst in red.

Boulevard				
Run	V_{par}	V_{per}	V_{perHV}	V_{J-J}
Neutral, 225°	0.268	0.288	0.318	0.285
Stable, 90°	0.171	0.214	0.198	0.168
Other street canyons				
Run	V_{par}	V_{per}	V_{perHV}	V_{J-J}
Neutral, 225°	0.099	0.110	0.130	0.104
Stable, 90°	0.081	0.095	0.102	0.083
Courtyards				
Run	V_{par}	V_{per}	V_{perHV}	V_{J-J}
Neutral, 225°	4.6×10^{-3}	3.0×10^{-3}	10.8×10^{-3}	16.6×10^{-3}
Stable, 90°	2.4×10^{-3}	2.5×10^{-3}	15.5×10^{-3}	2.6×10^{-3}
Surroundings				
Run	V_{par}	V_{per}	V_{perHV}	V_{J-J}
Neutral, 225°	0.039	0.046	0.056	0.037
Stable, 90°	0.020	0.030	0.029	0.021

D is calculated as

$$D(t,x,y,z) = \frac{\partial pc(t,x,y,z)}{\partial t} \approx \frac{pc(t+\Delta t,x,y,z) - pc(t,x,y,z)}{\Delta t}, \qquad (22)$$

where t and $t + \Delta t$ are two consecutive time steps. The higher D, the higher ventilation. According to the scalar conservation equation (e.g. Equation 11), D should be equal to the advective and turbulent transport terms.

D is calculated from the data output 3 over the large data output domain with a time step of 5 s inside an air volume below 20 m AGL. First, to minimize the dependence of D on the initial particle concentration when the source is switched off, the initial total particle concentration values $pc_{tot}(t = 0)$ inside the analysis domain in each version are normalized relative to that of V_{par}. Then, the time series of the volume averaged D can be calculated as follows:

$$\langle D(t)\rangle_V = \frac{\int_V D_N(t,x,y,z)dV}{\int_V dV}, \qquad (23)$$

where $D_N(x,y,z,t)$ is the dilution rate calculated using the normalized pc values. In order to study the horizontal variation of D inside the analysis domain, the

time average of D within each 2 m × 2 m × 20 m vertical column is calculated as

$$\langle D(x,y)\rangle_{z,t} = \frac{\int_t \int_z D_N(t,x,y,z)dzdt}{\int_t \int_z dzdt}. \tag{24}$$

Furthermore, the dilution of particles is observed to occur faster than expected as the total particle concentrations drop to half in about 120 s. Hence, only the first 75 s of the 5-min long data output 3 are selected for the analysis.

$\langle D(t)\rangle_V$ for both the neutral (a) and stable (b) runs is illustrated in Figure 16. All values are given relative to $\langle D(t)\rangle_V$ in $\mathrm{V_{par}}$. $\langle D(t)\rangle_V$ is highly variable with time in all city block design versions. As for the neutral runs, a clear distinction between $\mathrm{V_{par}}$, $\mathrm{V_{perHV}}$ and $\mathrm{V_{J-J}}$ is difficult to perceive whereas $\langle D(t)\rangle_V$ in $\mathrm{V_{per}}$ is systematically lower. For the stable runs, $\langle D(t)\rangle_V$ in $\mathrm{V_{per}}$ and $\mathrm{V_{J-J}}$ varies between being higher and lower than in $\mathrm{V_{par}}$, whereas $\mathrm{V_{perHV}}$ has almost constantly higher values than $\mathrm{V_{par}}$.

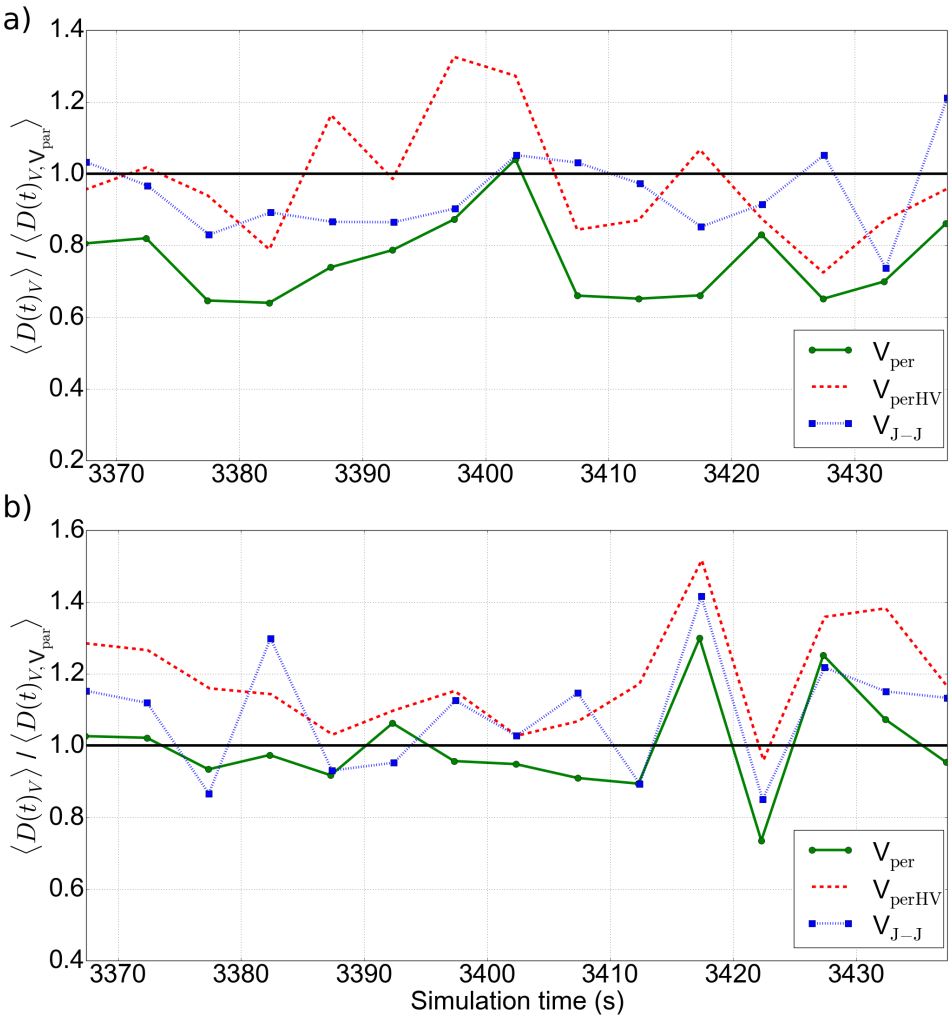

Figure 16: The volume averaged particle dilution rate $\langle D_V \rangle$ ($\mathrm{m^{-3}\,s^{-1}}$) below the height of $z = 20$ m : a) the neutral runs with $WD = 225$ ° and b) the stable runs with $WD = 90$ °. Results are represented relative to $\mathrm{V_{par}}$ ($\langle D_{V,\mathrm{V_{par}}} \rangle$).

Figure 17 illustrates $\langle D(x,y)\rangle_{z,t}$ for both the neutral (a) and stable (b) runs. If the initial concentration inside a column is zero, e.g. upwind of the particle source areas, $\langle D(x,y)\rangle_{z,t}$ cannot be calculated and it gets a NaN-value. In general, values are manifold for the neutral runs compared to the stable runs. Furthermore, $\langle D(x,y)\rangle_{z,t}$ decreases downwind as the columns further downstream receive particles also from the columns upstream. This advective nature of $\langle D(x,y)\rangle_{z,t}$ mostly explains the differences with the horizontal distribution of $F_{p,LF}$ in Figure 15. As for the neutral runs, clear differences in $\langle D(x,y)\rangle_{z,t}$ can be seen. Values appear to be highest in $\mathrm{V_{par}}$ and lowest in $\mathrm{V_{per}}$. Along the boulevard, $\langle D(x,y)\rangle_{z,t}$ is weaker in $\mathrm{V_{J-J}}$ compared to $\mathrm{V_{par}}$ and in $\mathrm{V_{per}}$ compared to $\mathrm{V_{perHV}}$. In $\mathrm{V_{par}}$, $\langle D(x,y)\rangle_{z,t}$ has high values especially in the southern part of the boulevard and at the major junction but low values in the northern end where $\mathrm{V_{J-J}}$ performs better instead. The relation between D and pc values can be seen, for instance, as lower pc north of the major junction and higher pc in the northern end of the boulevard in $\mathrm{V_{par}}$ than in $\mathrm{V_{J-J}}$ (see Figure 12). In $\mathrm{V_{perHV}}$, also the smaller streets west of the boulevard have high values of $\langle D(x,y)\rangle_{z,t}$. For the stable runs, $\langle D(x,y)\rangle_{z,t}$ is high south of the major junction but low north of the major junction in $\mathrm{V_{par}}$ whereas in $\mathrm{V_{J-J}}$, the pattern is more complex. $\langle D(x,y)\rangle_{z,t}$ is higher in $\mathrm{V_{perHV}}$ than $\mathrm{V_{per}}$, and high values are observed further downstream as well. In both the neutral and stable runs, surprising details can be seen when focusing on the courtyards. For example, on the eastern side of the major junction, the courtyards have very different $\langle D(x,y)\rangle_{z,t}$ values when comparing $\mathrm{V_{par}}$ with $\mathrm{V_{J-J}}$ and $\mathrm{V_{per}}$ with $\mathrm{V_{perHV}}$.

Horizontal mean values of $\langle D(x,y)\rangle_{z,t}$ separately for the boulevard, the other street canyons, the courtyards and the surroundings are given in Table 4. For the neutral runs, values are highest in $\mathrm{V_{par}}$ in all parts except for the other street canyons where $\mathrm{V_{J-J}}$ performs best. Lowest values are observed in $\mathrm{V_{per}}$ everywhere except along the boulevard where $\mathrm{V_{perHV}}$ performs worst. For stable runs, mean $\langle D(x,y)\rangle_{z,t}$ is highest inside the courtyards in $\mathrm{V_{per}}$ and in $\mathrm{V_{perHV}}$ elsewhere. $\mathrm{V_{par}}$ has a low value along the boulevard, which is not obvious in Figure 17b. Lowest values are observed along the boulevard in $\mathrm{V_{par}}$, inside the other street canyons in $\mathrm{V_{per}}$ and inside the courtyards and in the surroundings in $\mathrm{V_{J-J}}$.

For the neutral runs, $\mathrm{V_{par}}$ and $\mathrm{V_{J-J}}$ perform best according to D, whereas for the stable runs $\mathrm{V_{per}}$ and $\mathrm{V_{perHV}}$ perform best. This shows that ventilation is higher when the flow is less blocked, which agrees with the results in Lo and Ngan (2015) and that D is governed by the horizontal advection. For instance in the neutral runs, $\mathrm{V_{par}}$ and $\mathrm{V_{J-J}}$ have long canyons in the wind direction which enables channelling whereas in $\mathrm{V_{per}}$ and $\mathrm{V_{perHV}}$ the canyons are shorter and flow structures related to building corners disturb the horizontal mean flow. Conversely

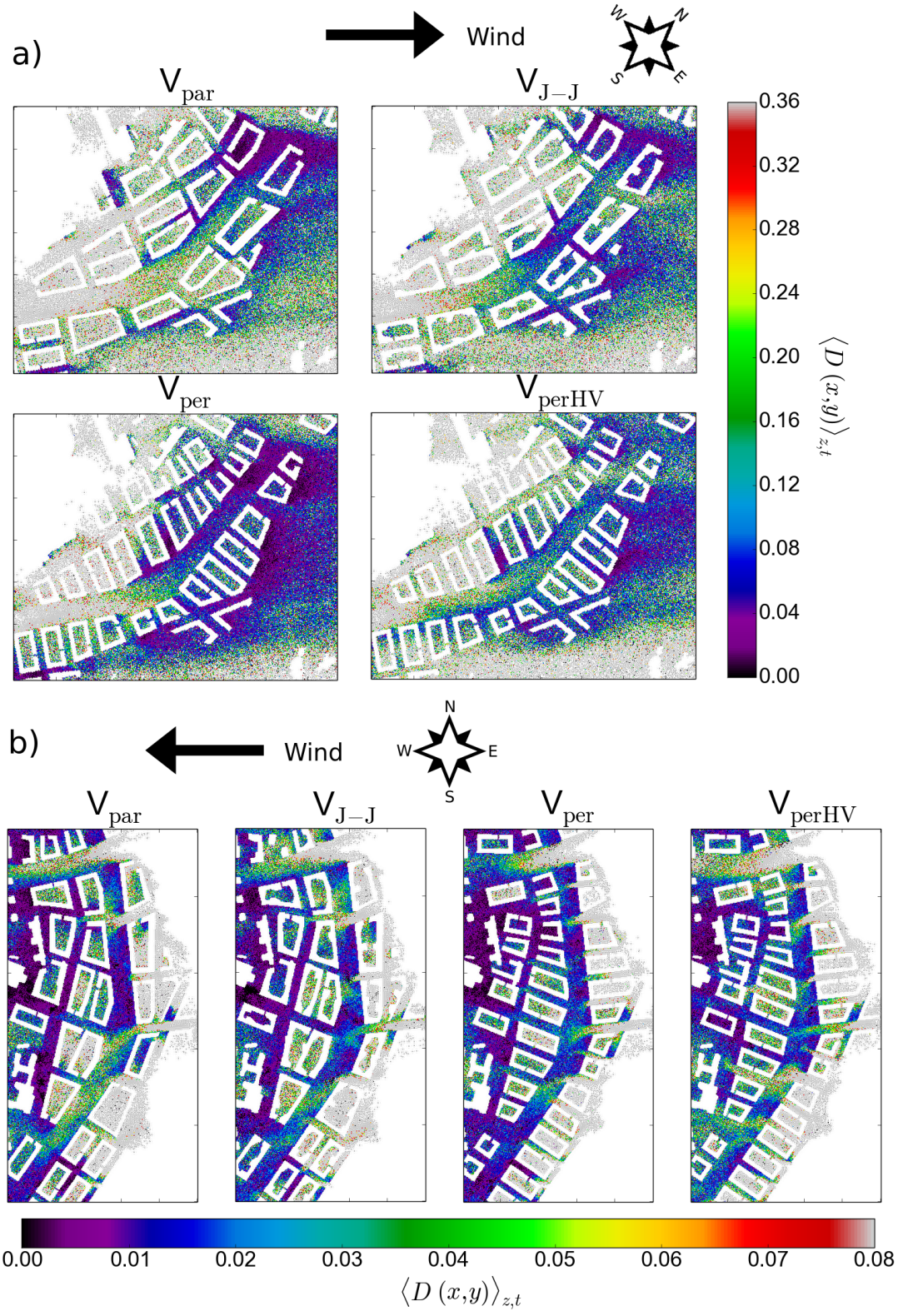

Figure 17: The temporal mean particle dilution rate $\langle D(x,y)\rangle_{z,t}$ ($\mathrm{m^{-3}\,s^{-1}}$) below the height of $z = 20$ m for the first 75 s after the particle source is switched off: a) the neutral runs with $WD = 225$ ° and b) the stable runs with $WD = 90$ °. NaN-values are given in white.

Table 4: Mean $\langle D(x,y)\rangle_{z,t}$ ($\mathrm{m^{-3}\,s^{-1}}$) separately for the boulevard, the other street canyons, the courtyards and the surroundings between heights of $z = 2$ m and $z = 20$ m for all runs. D is calculated using data from the first 75 s after the particle source has been switched off.

Boulevard				
Stability and *WD*	V_{par}	V_{per}	V_{perHV}	V_{J-J}
Neutral, 225°	1.97	1.22	0.70	1.00
Stable, 90°	0.08	0.09	0.17	0.10
Other street canyons				
Stability and *WD*	V_{par}	V_{per}	V_{perHV}	V_{J-J}
Neutral, 225°	1.25	0.76	1.06	1.41
Stable, 90°	0.68	0.60	0.72	0.63
Courtyards				
Stability and *WD*	V_{par}	V_{per}	V_{perHV}	V_{J-J}
Neutral, 225°	1.56	0.79	0.88	1.35
Stable, 90°	0.77	1.03	0.94	0.71
Surroundings				
Stability and *WD*	V_{par}	V_{per}	V_{perHV}	V_{J-J}
Neutral, 225°	1.24	0.60	1.20	1.10
Stable, 90°	0.59	0.48	0.66	0.45

for the stable runs, the volume of street canyons parallel to the wind direction is larger in V_{per} and V_{perHV}.

6 Discussion

A high-resolution LES study over a real urban surface is conducted in order to compare pollutant ventilation and dispersion inside street canyons and courtyards in four alternative city block design versions. The results suggest that the distinctly different characteristics of the design versions can result in notably dissimilar particle concentration patterns and ventilation capacities.

The main goal of this study is to give a comparison of the alternative design versions, and this way provide important information to urban planners and decision makers about the impact on urban planning on local air quality. Hence, a suggestive ranking based on the results in Section 5 is performed. The performance of each version is rated on a relative scale 0 - 1 based on each measure applied in the analysis in the following way

$$z_{\mathrm{type}} = \frac{x_{\mathrm{type}} - \min(x)}{\max(x) - \min(x)}, \tag{25}$$

where x_{type} is the mean value and z_{type} is the normalised mean value for each city

block design type inside the boulevard, the other street canyons, the courtyards or in the surroundings. As for *pc*, an average grade is given based on both the mean and 90th percentile values at both analysis levels. Furthermore, the normalized value is calculated as 1 - z_{type} since lower *pc* indicates better air quality. As for $\langle D_V \rangle$, an extra (minus) 0.5 point is given if a version performs clearly better (weaker) compared to the other versions.

a)

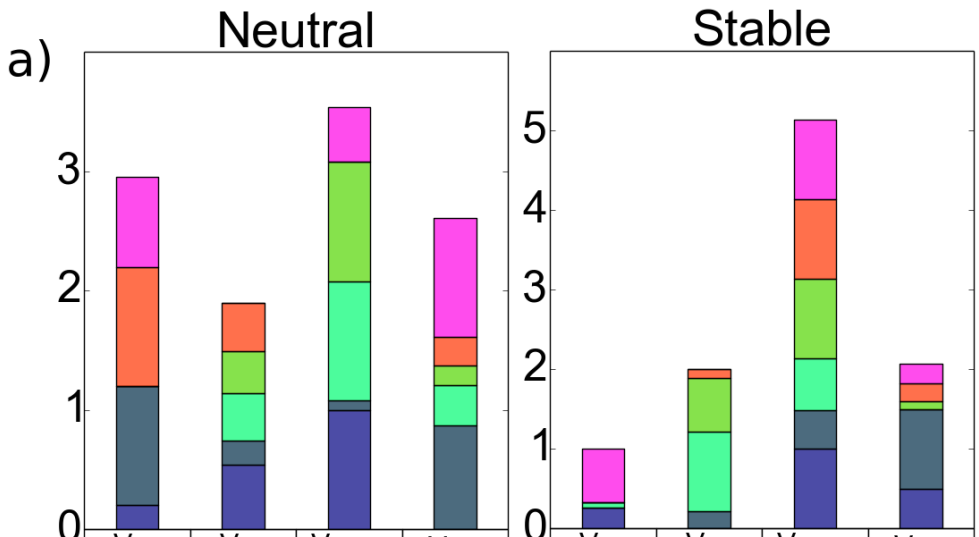

b)

	V_{par}	V_{per}	V_{perHV}	V_{J-J}	V_{par}	V_{per}	V_{perHV}	V_{J-J}
pc: B	0.20	0.54	1.00	0.00	0.26	0.00	1.00	0.50
pc: O	1.00	0.20	0.08	0.87	0.00	0.22	0.49	1.00
pc: C	1.00	0.81	0.48	0.00	1.00	0.58	0.00	0.53
pc: S	1.00	0.00	0.53	0.88	1.00	0.00	0.77	0.95
F_p: B	0.00	0.40	1.00	0.34	0.07	1.00	0.65	0.00
F_p: O	0.00	0.35	1.00	0.16	0.00	0.67	1.00	0.10
F_p: C	0.12	0.00	0.57	1.00	0.00	0.01	1.00	0.02
F_p: S	0.11	0.47	1.00	0.00	0.00	1.00	0.90	0.10
$\langle D_V \rangle$	0.00	-0.50	0.00	0.00	0.00	0.00	0.50	0.00
$\langle D(x,y) \rangle_{z,t}$: B	1.00	0.41	0.00	0.24	0.00	0.11	1.00	0.22
$\langle D(x,y) \rangle_{z,t}$: O	0.75	0.00	0.46	1.00	0.67	0.00	1.00	0.25
$\langle D(x,y) \rangle_{z,t}$: C	1.00	0.00	0.12	0.73	0.19	1.00	0.72	0.00
$\langle D(x,y) \rangle_{z,t}$: S	1.00	0.00	0.94	0.78	0.67	0.14	1.00	0.00
SUM	7.18	2.68	7.18	6.00	3.86	4.73	10.03	3.67

Figure 18: Ranking of the performance of each version (V_{par}, V_{per}, V_{perHV} and V_{J-J}) based on each analysis measure for both the neutral and stable runs. The scale is 0-1 with 1 being the best. B = Boulevard, O = Other street canyons, C = Courtyards and S = Surroundings. Ranking only for the street canyons is illustrated in a) whereas all points are shown in b). The colours in the bar plot a) correspond to colours in the table b).

Figure 18 illustrates the ranking for both meteorological conditions applied in the simulations. All the points given considering all part of the analysis do-

main are displayed in Figure 18b. For the neutral runs, V_{per} achieves the lowest total points whereas both V_{par} and V_{perHV} achieve the highest. V_{par} achieves high points especially based on *pc* and D, but on the other hand, F_p is weakest in V_{par}. V_{perHV} ranks best based on F_p. Along the boulevard, V_{perHV} performs best whereas the highest points inside the other street canyons and the courtyards are achieved by V_{J-J} and V_{par}, respectively. As for the stable runs, the outperformance of V_{perHV} is notable with over 5 points difference to the other versions. Similar to the neutral runs, V_{perHV} achieves highest points based on F_p but also on D. Contrary to the neutral runs, V_{par} performs worst in stable conditions. Again, V_{par} achieves lowest points based on F_p, which suggests that F_p is strongly determined by the urban topography. Furthermore, D depends highly on the wind direction as it is shown to be governed by the horizontal advection and the volume of street canyons parallel to the wind direction. Hence, both turbulent and advective transport of particles are assessed in this study.

Furthermore, *pc* values inside the courtyards remain relatively low throughout the simulation, which is naturally a good aspect. On the other hand, this shifts the focus of the ranking on the street canyons and especially on the boulevard where the number of pedestrians being exposed to pollutants is highest. If only the street canyons are considered (Figure 18a), V_{perHV} performs best in both meteorological conditions and the outperformance is especially pronounced for the stable runs.

Hence, this ranking suggests that V_{perHV} with the longest side of the buildings perpendicular to the boulevard and with a varying roof height is the best choice when it comes to ventilation of street canyons and courtyards under two contrasting meteorological conditions. Thereafter, the distinction between V_{par}, V_{per} and V_{J-J} is not that evident, especially in neutral conditions. In stable conditions, V_{J-J} performs slightly better along the boulevard. According to the ranking, none of the versions is clearly weakest. This result agrees with those of the previous studies showing that variability in the building height enhances dispersion and ventilation of pollutants over an urban surface (Hoydysh et al., 1974; Gu et al., 2011; Lo and Ngan, 2015; Nosek et al., 2016).

On the other hand, irregularities in the building shape in V_{J-J} do not result in any notable improvements according to the results. The irregularities probably destroy the canyon vortex, which reduces the air exchange rate and re-entrainment of pollutants to the street canyons (Yang et al., 2016), while ventilation by turbulent transport may decrease simultaneously. Further in-depth studies are needed to explain the last-mentioned result.

Applying a high-resolution LES model over a real topography of a vast extent provides a large amount of explicit information about the flow field above

the area of interest. However, the amount of data output is very high and the complexity of the topography further complicates the analysis. Thus, choosing simple measures of ventilation capacity for a comparative study is rather difficult. Therefore, in this study, the ranking of alternative city block design versions is chosen to be based upon the horizontal mean values of the measures applied in the analysis. Hence, the horizontal variance and the impact of single pollutant hot-spots is faded. These details should be considered, for example, when planning the exact locations of street-levels cafés and shops. Moreover, the number of different meteorological conditions applied in the simulations was limited to two due to the high computational expenses of the simulations. However, they were chosen carefully to represent the most frequent conditions as well as the conditions that typically lead to poor air quality events in Helsinki. Last of all, only the aerodynamic impacts of both buildings and trees are taken into account in this study and for instance the role of heat fluxes or chemistry is omitted.

7 Summary and conclusions

This study aims at comparing pollutant ventilation and dispersion inside street canyons and courtyards in four alternative city block design versions. The study area is one of the city boulevards planned to be built in the City Plan of Helsinki for 2050. A high-resolution numerical simulation applying a LES model PALM embedded with a Lagrangian stochastic particle and a plant canopy models is conducted over a real urban surface under two different meteorological conditions. The objective is to provide urban planners and decision makers vital information on the impact of urban morphology on the air quality by ranking the alternative city block design versions. This is done according to their capability to transport traffic-related pollutants away from the pedestrian level.

The numerical simulations in this study apply many highly developed features of PALM, such as the full three-dimensional two-way self-nesting, which is utilized for the first time. Moreover, the embedded Lagrangian particle and the canopy model are revised in order to take into account the horizontal heterogeneity of particle sources as well as the location of trees both along the boulevard and in the surroundings.

The analysis is based on comparing the 40-min temporal mean particle concentrations (pc), the turbulent vertical particle flux densities (F_p) and the particle dilution rate (D). All these measures of ventilation capacity show strong dependence on both the urban morphology and meteorological conditions. Variability in the building height and shape as well as the length of the canyon are shown to modify the accumulation of pc inside street canyons and thus also F_p above them.

Despite the closeness of the particle sources, the courtyards by the boulevard remain relatively clean. Hence, F_p above the courtyards is close to zero or even negative while F_p is highest above the source areas i.e. streets. In spite of equal particle release rates, clear differences in F_p between the different design versions can be observed. D is governed by the horizontal advection and is thus related to the volume of street canyons parallel to the wind direction. F_p measures only turbulent transport whereas D includes the advective transport as well, which explains the differences between these two measures.

Horizontal mean values of pc, F_p and D (both volume and column averaged) inside each design version both for the neutral and stable runs are calculated separately for the boulevard, the other street canyons, the courtyards and the surroundings that does not include to the streets or the courtyards. A suggestive ranking is performed by grading the performance of each version based on each measure. Focusing on the street canyons and especially the boulevard suggests that $\mathrm{V_{perHV}}$ with a varying roof height and the longest side of the buildings perpendicular to the boulevard would be the best option regarding the ventilation capacity of the street canyons, especially in meteorological conditions that often lead to the worst air quality events in Helsinki. Previous studies on the impact of roof height variability on the ventilation of street canyons support the results. However, the relatively low performance of $\mathrm{V_{J-J}}$ with an irregular building shape was not expected.

This is the first LES study over a real urban topography applying sophisticated measures to assess pollutant dispersion and ventilation inside street canyons and courtyards. The numerical methods employed in PALM are novel and highly developed. The results provide with unique information about the transport of traffic-related pollutants in this specific urban environment and the results can directly be applied by local urban planners. Yet, a pleasant urban living environment is an outcome of many different factors that counteract each other. For instance, strong gusts and canalizing of wind transport pollutants efficiently but result in an uncomfortably windy environment for a pedestrian. Furthermore, street trees are important for thermal comfort by proving with shade but at the same time they can increase pollutant concentrations locally by blocking the air flow. On top of controlling air quality, noise pollution should be avoided as well. Therefore, reconciling and weighting of different aforementioned aspects are needed in city planning and decision making.

Acknowledgements

This master's thesis is one part of a project commissioned and funded by the City Planning Department of the City of Helsinki. I want to thank the whole project team there and especially Christina Suomi for the project management and Tapani Rauramo, Jari Rantsi and Pihla Melander for their active cooperation concerning the urban morphology and traffic data. Above all, I want to thank my supervisors Leena Järvi, Antti Hellsten, Mikko Auvinen and Timo Vesala for their guidance and great support during this process as well as for reviewing the thesis.

References

Amorim, J. H., J. Valente, P. Cascão, V. Rodrigues, C. Pimentel, A. I. Miranda, and C. Borrego, 2013: Pedestrian exposure to air pollution in cities: Modeling the effect of roadside trees. *Advances in Meteorology*, doi:http://dx.doi.org/10.1155/2013/964904.

Arya, S., 2001: *Introduction to Micrometeorology*. International geophysics series, Academic Press.

Baik, J.-J., and J.-J. Kim, 2002: On the escape of pollutants from urban street canyons. *Atmospheric Environment*, **36 (3)**, 527 – 536, doi:http://dx.doi.org/10.1016/S1352-2310(01)00438-1, URL http://www.sciencedirect.com/science/article/pii/S1352231001004381, seventh Internatioonal Conference on Atmospheric Science and Applications to Air Quality (ASAAQ).

Basu, S., and F. Porté-Agel, 2006: Large-eddy simulation of stably stratified atmospheric boundary layer turbulence: A scale-dependent dynamic modeling approach. *Journal of the Atmospheric Sciences*, **63 (8)**, 2074–2091, doi:10.1175/JAS3734.1, URL http://dx.doi.org/10.1175/JAS3734.1.

Beare, R. J., and Coauthors, 2006: An intercomparison of large-eddy simulations of the stable boundary layer. *Boundary-Layer Meteorology*, **118 (2)**, 247–272, doi:10.1007/s10546-004-2820-6, URL http://dx.doi.org/10.1007/s10546-004-2820-6.

Bentham, T., and R. Britter, 2003: Spatially averaged flow within obstacle arrays. *Atmospheric Environment*, **37 (15)**, 2037 – 2043, doi:http://dx.doi.org/10.1016/S1352-2310(03)00123-7, URL http://www.sciencedirect.com/science/article/pii/S1352231003001237.

Berselli, L., T. Iliescu, and W. Layton, 2006: *Mathematics of Large Eddy Simulation of Turbulent Flows*. Scientific Computation, Springer.

Blocken, B., 2015: Computational fluid dynamics for urban physics: Importance, scales, possibilities, limitations and ten tips and tricks towards accurate and reliable simulations. *Building and Environment*, **91**, 219 – 245, doi:http://dx.doi.org/10.1016/j.buildenv.2015.02.015, URL http://www.sciencedirect.com/science/article/pii/S0360132315000724, fifty Year Anniversary for Building and Environment.

Britter, R. E., and S. R. Hanna, 2003: Flow and dispersion in urban areas. *Annual Review of Fluid Mechanics*, **35 (1)**, 469–496, doi:10.1146/annurev.fluid.35.101101.161147, URL http://dx.doi.org/10.1146/annurev.fluid.35.101101.161147.

Brunekreef, B., and S. T. Holgate, 2002: Air pollution and health. *The Lancet*, **360 (9341)**, 1233 – 1242, doi:http://dx.doi.org/10.1016/S0140-6736(02)11274-8, URL http://www.sciencedirect.com/science/article/pii/S0140673602112748.

Buccolieri, R., C. Gromke, S. D. Sabatino, and B. Ruck, 2009: Aerodynamic effects of trees on pollutant concentration in street canyons. *Science of The Total Environment*, **407 (19)**, 5247 – 5256, doi:http://dx.doi.org/10.1016/j.scitotenv.2009.06.016, URL http://www.sciencedirect.com/science/article/pii/S0048969709005944.

Buccolieri, R., M. Sandberg, and S. D. Sabatino, 2010: City breathability and its link to pollutant concentration distribution within urban-like geometries. *Atmospheric Environment*, **44 (15)**, 1894 – 1903, doi:http://dx.doi.org/10.1016/j.atmosenv.2010.02.022, URL http://www.sciencedirect.com/science/article/pii/S1352231010001391.

Cai, X.-M., 2012: Effects of wall heating on flow characteristics in a street canyon. *Boundary-Layer Meteorology*, **142 (3)**, 443–467.

Cai, X.-M., J. Barlow, and S. Belcher, 2008: Dispersion and transfer of passive scalars in and above street canyons—Large-eddy simulations. *Atmospheric Environment*, **42 (23)**, 5885 – 5895, doi:http://dx.doi.org/10.1016/j.atmosenv.2008.03.040, URL http://www.sciencedirect.com/science/article/pii/S1352231008003051.

Cassiani, M., G. G. Katul, and J. D. Albertson, 2008: The effects of canopy leaf area index on airflow across forest edges: Large-eddy simulation and an-

alytical results. *Boundary-Layer Meteorology*, **126 (3)**, 433–460, doi:10.1007/s10546-007-9242-1, URL http://dx.doi.org/10.1007/s10546-007-9242-1.

Cheng, W., and C.-H. Liu, 2011: Large-eddy simulation of turbulent transports in urban street canyons in different thermal stabilities. *Journal of Wind Engineering and Industrial Aerodynamics*, **99 (4)**, 434 – 442, doi:http://dx.doi.org/10.1016/j.jweia.2010.12.009, URL http://www.sciencedirect.com/science/article/pii/S016761051000142X, the Fifth International Symposium on Computational Wind Engineering.

Christen, A., 2005: Atmospheric turbulence and surface energy exchange in urban environments: results from the Basel Urban Boundary Layer Experiment (BUBBLE). Ph.D. thesis, University of Basel.

City Planning Department, City of Helsinki, 2015: City boulevards in Helsinki. URL http://www.hel.fi/hel2/ksv/julkaisut/esitteet/esite_2015-4_en.pdf.

Dabberdt, W. F., and W. G. Hoydysh, 1991: Street canyon dispersion: Sensitivity to block shape and entrainment. *Atmospheric Environment. Part A. General Topics*, **25 (7)**, 1143 – 1153, doi:http://dx.doi.org/10.1016/0960-1686(91)90225-V, URL http://www.sciencedirect.com/science/article/pii/096016869190225V.

Deardorff, J. W., 1980: Stratocumulus-capped mixed layers derived from a three-dimensional model. *Boundary-Layer Meteorology*, **18 (4)**, 495–527, doi:10.1007/BF00119502, URL http://dx.doi.org/10.1007/BF00119502.

Dupont, S., and Y. Brunet, 2008: Edge flow and canopy structure: A large-eddy simulation study. *Boundary-Layer Meteorology*, **126 (1)**, 51–71, doi:10.1007/s10546-007-9216-3, URL http://dx.doi.org/10.1007/s10546-007-9216-3.

Finnigan, J., 2000: Turbulence in plant canopies. *Annual Review of Fluid Mechanics*, **32 (1)**, 519–571, doi:10.1146/annurev.fluid.32.1.519, URL http://dx.doi.org/10.1146/annurev.fluid.32.1.519.

Foken, T., 2008: *Micrometeorology*. Springer, Berlin, Heidelberg, 1–24 pp., doi:10.1007/978-3-540-74666-9_4, URL http://dx.doi.org/10.1007/978-3-540-74666-9_4.

Giometto, M. G., A. Christen, C. Meneveau, J. Fang, M. Krafczyk, and M. B. Parlange, 2016: Spatial characteristics of roughness sublayer mean flow and turbulence over a realistic urban surface. *Boundary-Layer Meteorology*, 1–28, doi:10.1007/s10546-016-0157-6, URL http://dx.doi.org/10.1007/s10546-016-0157-6.

Gousseau, P., B. Blocken, T. Stathopoulos, and G. van Heijst, 2015: Near-field pollutant dispersion in an actual urban area: Analysis of the mass transport mechanism by high-resolution large eddy simulations. *Computers & Fluids*, **114**, 151 – 162, doi:http://dx.doi.org/10.1016/j.compfluid.2015.02.018, URL http://www.sciencedirect.com/science/article/pii/S0045793015000614.

Groenendijk, M., and Coauthors, 2011: Seasonal variation of photosynthetic model parameters and leaf area index from global Fluxnet eddy covariance data. *Journal of Geophysical Research: Biogeosciences*, **116 (G4)**, n/a–n/a, doi:10.1029/2011JG001742, URL http://dx.doi.org/10.1029/2011JG001742, g04027.

Gromke, C., and B. Blocken, 2015: Influence of avenue-trees on air quality at the urban neighborhood scale. Part II: Traffic pollutant concentrations at pedestrian level. *Environmental Pollution*, **196**, 176 – 184, doi:http://dx.doi.org/10.1016/j.envpol.2014.10.015, URL http://www.sciencedirect.com/science/article/pii/S0269749114004382.

Gromke, C., and B. Ruck, 2009: On the impact of trees on dispersion processes of traffic emissions in street canyons. *Boundary-Layer Meteorology*, **131 (1)**, 19–34, doi:10.1007/s10546-008-9301-2, URL http://dx.doi.org/10.1007/s10546-008-9301-2.

Gu, Z., Y. Zhang, and K. Lei, 2010: Large eddy simulation of flow in a street canyon with tree planting under various atmospheric instability conditions. *Science China Technological Sciences*, **53 (7)**, 1928–1937, doi:10.1007/s11431-010-3243-x, URL http://dx.doi.org/10.1007/s11431-010-3243-x.

Gu, Z.-L., Y.-W. Zhang, Y. Cheng, and S.-C. Lee, 2011: Effect of uneven building layout on air flow and pollutant dispersion in non-uniform street canyons. *Building and Environment*, **46 (12)**, 2657 – 2665, doi:http://dx.doi.org/10.1016/j.buildenv.2011.06.028, URL http://www.sciencedirect.com/science/article/pii/S0360132311002083.

Heiskanen, J., M. Rautiainen, P. Stenberg, M. Mõttus, V.-H. Vesanto, L. Korhonen, and T. Majasalmi, 2012: Seasonal variation in MODIS LAI for a boreal forest area in Finland. *Remote Sensing of Environment*, **126**, 104 – 115, doi:http://dx.doi.org/10.1016/j.rse.2012.08.001, URL http://www.sciencedirect.com/science/article/pii/S0034425712003021.

Hellsten, A., K. Ketelsen, F. Barmpas, G. Tsegas, N. Moussiopoulos, and S. Raasch, 2016: Nested multi-scale system in the PALM large-eddy simulation model [accepted extended abstract]. *Proceedings of the 34th International*

Technical Meeting on Air Pollution Modelling and its Application, 3-7 October, 2016, Chania, Crete, Greece, NATO-CCMS.

Hellsten, A., and Coauthors, 2015: Footprint evaluation for flux and concentration measurements for an urban-like canopy with coupled Lagrangian stochastic and large-eddy simulation models. *Boundary-Layer Meteorology*, **157 (2)**, 191–217, doi:10.1007/s10546-015-0062-4.

Holmes, N., and L. Morawska, 2006: A review of dispersion modelling and its application to the dispersion of particles: An overview of different dispersion models available. *Atmospheric Environment*, **40 (30)**, 5902 – 5928, doi:http://dx.doi.org/10.1016/j.atmosenv.2006.06.003, URL http://www.sciencedirect.com/science/article/pii/S1352231006006339.

Holton, J. R., 1992: Chapter 5 - the planetary boundary layer. *An Introduction to Dynamic Meteorology*, J. R. HOLTON, Ed., International Geophysics, Vol. 48, Academic Press, 116 – 140, doi:http://dx.doi.org/10.1016/B978-0-12-354355-4.50009-7, URL http://www.sciencedirect.com/science/article/pii/B9780123543554500097.

Hoydysh, G. W., A. R. Griffiths, and Y. Ogawa, 1974: A scale model study of the dispersion of pollution in street canyons. *67th Annual meeting of the Air Pollution Control Association.*

Hoydysh, W. G., and W. F. Dabberdt, 1988: Kinematics and dispersion characteristics of flows in asymmetric street canyons. *Atmospheric Environment (1967)*, **22 (12)**, 2677 – 2689, doi:http://dx.doi.org/10.1016/0004-6981(88)90436-2, URL http://www.sciencedirect.com/science/article/pii/0004698188904362.

Idczak, M., P. Mestayer, J.-M. Rosant, J.-F. Sini, and M. Violleau, 2007: Micrometeorological measurements in a street canyon during the joint ATREUS-PICADA experiment. *Boundary-Layer Meteorology*, **124 (1)**, 25–41.

Janhäll, S., 2015: Review on urban vegetation and particle air pollution – Deposition and dispersion. *Atmospheric Environment*, **105**, 130 – 137, doi:http://dx.doi.org/10.1016/j.atmosenv.2015.01.052, URL http://www.sciencedirect.com/science/article/pii/S1352231015000758.

Kanani-Sühring, F., and S. Raasch, 2015: Spatial variability of scalar concentrations and fluxes downstream of a clearing-to-forest transition: A large-eddy simulation study. *Boundary-Layer Meteorology*, **155 (1)**, 1–27, doi:10.1007/s10546-014-9986-3, URL http://dx.doi.org/10.1007/s10546-014-9986-3.

Kanda, M., A. Inagaki, T. Miyamoto, M. Gryschka, and S. Raasch, 2013: A new aerodynamic parametrization for real urban surfaces. *Boundary-Layer Meteorology*, **148 (2)**, 357–377, doi:10.1007/s10546-013-9818-x, URL http://dx.doi.org/10.1007/s10546-013-9818-x.

Karsisto, P., C. Fortelius, M. Demuzere, C. S. B. Grimmond, K. W. Oleson, R. Kouznetsov, V. Masson, and L. Järvi, 2016: Seasonal surface urban energy balance and wintertime stability simulated using three land-surface models in the high-latitude city Helsinki. *Quarterly Journal of the Royal Meteorological Society*, **142 (694)**, 401–417, doi:10.1002/qj.2659, URL http://dx.doi.org/10.1002/qj.2659.

Kataoka, H., and M. Mizuno, 2002: Numerical flow computation around aeroelastic 3D square cylinder using inflow turbulence. *Wind and Structures*, **5 (2-4)**, 397–392, doi:10.12989/was.2002.5.2_3_4.379.

Keck, M., S. Raasch, M. O. Letzel, and E. Ng, 2014: First results of high resoltuion large-eddy simulations of the atmospheric boundary layer. *Journal of Heat Island Institute International*, **9 (2)**, 39–43.

Kikuchi, A., N. Hataya, A. Mochida, H. Yoshino, Y. Tabata, H. Watanabe, and Y. Jyunimura, 2007: Field study of the influences of roadside trees and moving automobiles on turbulent diffusion of air pollutant and thermal environment in urban street canyons. *Proceedings of the 6th International Conference on Indoor Air Quality, Ventilation and Energy Conservation in Buildings, Sendai, Japan, 28-31 October 2007*, Air Infilitration and Ventilation Centre, Brussels, Belgium.

Kikumoto, H., R. Ooka, and K. Uehara, 2009: Large-eddy simulation of gaseous diffusion in street canyon with thermal stratification. *The seventh Asia-Pacific conference on wind engineering*, Taipei, Taiwan.

Kim, Y., L. Huang, S. Gong, and C. Q. Jia, 2016: A new approach to quantifying vehicle induced turbulence for complex traffic scenarios. *Chinese Journal of Chemical Engineering*, **24 (1)**, 71 – 78, doi:http://dx.doi.org/10.1016/j.cjche.2015.11.025, URL http://www.sciencedirect.com/science/article/pii/S1004954115004346, special issue of Chinese Journal of Chemical Engineering in memory of Professor Mooson Kwauk.

Kimm, H., and Y. Ryu, 2015: Seasonal variations in photosynthetic parameters and leaf area index in an urban park. *Urban Forestry & Urban Greening*, **14 (4)**, 1059 – 1067, doi:http://dx.doi.org/10.1016/j.ufug.2015.10.003, URL http://www.sciencedirect.com/science/article/pii/S1618866715001399.

Kurppa, M., A. Nordbo, S. Haapanala, and L. Järvi, 2015: Effect of seasonal variability and land use on particle number and CO2 exchange in Helsinki, Finland. *Urban Climate*, **13**, 94 – 109, doi:http://dx.doi.org/10.1016/j.uclim.2015.07.006, URL http://www.sciencedirect.com/science/article/pii/S2212095515300122.

Lee, Y. S., and J. J. Kim, 2009: A CFD modelling on the effect of building density on urban flow. *The 7th International Conference on Urban Climate, Yokohama*.

Letzel, M. O., C. Helmke, E. Ng, X. An, A. Lai, and S. Raasch, 2012: LES case study on pedestrian level ventilation in two neighbourhoods in Hong Kong. *Meteorologische Zeitschrift*, **21 (6)**, 575–589.

Letzel, M. O., M. Krane, and S. Raasch, 2008: High resolution urban large-eddy simulation studies from street canyon to neighbourhood scale. *Atmospheric Environment*, **42 (38)**, 8770 – 8784, doi:http://dx.doi.org/10.1016/j.atmosenv.2008.08.001, URL http://www.sciencedirect.com/science/article/pii/S1352231008007036.

Li, X.-X., C.-H. Liu, and D. Y. Leung, 2009: Numerical investigation of pollutant transport characteristics inside deep urban street canyons. *Atmospheric Environment*, **43 (15)**, 2410 – 2418, doi:http://dx.doi.org/10.1016/j.atmosenv.2009.02.022, URL http://www.sciencedirect.com/science/article/pii/S1352231009001198.

Li, X.-X., C.-H. Liu, D. Y. Leung, and K. Lam, 2006: Recent progress in CFD modelling of wind field and pollutant transport in street canyons. *Atmospheric Environment*, **40 (29)**, 5640 – 5658, doi:http://dx.doi.org/10.1016/j.atmosenv.2006.04.055, URL http://www.sciencedirect.com/science/article/pii/S1352231006004559.

Liu, C., D. Leung, and M. Barth, 2005: On the prediction of air and pollutant exchange rates in street canyons of different aspect ratios using large-eddy simulation. *Atmospheric Environment*, **39 (9)**, 1567–1574.

Liu, C.-H., M. C. Barth, and D. Y. C. Leung, 2004: Large-eddy simulation of flow and pollutant transport in street canyons of different building-height-to-street-width ratios. *Journal of Applied Meteorology*, **43 (10)**, 1410–1424, doi:10.1175/JAM2143.1, URL http://dx.doi.org/10.1175/JAM2143.1.

Liu, C.-H., W. Cheng, T. C. Leung, and D. Y. Leung, 2011: On the mechanism of air pollutant re-entrainment in two-dimensional idealized street canyons. *At-*

mospheric Environment, **45 (27)**, 4763 – 4769, doi:http://dx.doi.org/10.1016/j.atmosenv.2010.03.015, URL http://www.sciencedirect.com/science/article/pii/S1352231010002104.

Liu, C.-H., C.-T. Ng, and C. C. Wong, 2015: A theory of ventilation estimate over hypothetical urban areas. *Journal of Hazardous Materials*, **296**, 9 – 16, doi:http://dx.doi.org/10.1016/j.jhazmat.2015.04.018, URL http://www.sciencedirect.com/science/article/pii/S0304389415003003.

Lo, K., and K. Ngan, 2015: Characterising the pollutant ventilation characteristics of street canyons using the tracer age and age spectrum. *Atmospheric Environment*, **122**, 611 – 621, doi:http://dx.doi.org/10.1016/j.atmosenv.2015.10.023, URL http://www.sciencedirect.com/science/article/pii/S135223101530443X.

Maronga, B., and Coauthors, 2015: The parallelized large-eddy simulation model (PALM) version 4.0 for atmospheric and oceanic flows: model formulation, recent developments, and future perspectives. *Geoscientific Model Development*, **8 (8)**, 2515–2551, doi:10.5194/gmd-8-2515-2015, URL http://www.geosci-model-dev.net/8/2515/2015/.

McCreanor, J., and Coauthors, 2007: Respiratory effects of exposure to diesel traffic in persons with asthma. *New England Journal of Medicine*, **357 (23)**, 2348–2358, doi:10.1056/NEJMoa071535, URL http://dx.doi.org/10.1056/NEJMoa071535, pMID: 18057337, http://dx.doi.org/10.1056/NEJMoa071535.

Michioka, T., H. Takimoto, and A. Sato, 2014: Large-eddy simulation of pollutant removal from a three-dimensional street canyon. *Boundary-Layer Meteorology*, **150 (2)**, 259–275, doi:10.1007/s10546-013-9870-6, URL http://dx.doi.org/10.1007/s10546-013-9870-6.

Mochida, A., and I. Y. Lun, 2008: Prediction of wind environment and thermal comfort at pedestrian level in urban area. *Journal of Wind Engineering and Industrial Aerodynamics*, **96 (10–11)**, 1498 – 1527, doi:http://dx.doi.org/10.1016/j.jweia.2008.02.033, URL http://www.sciencedirect.com/science/article/pii/S0167610508000287, 4th International Symposium on Computational Wind Engineering (CWE2006).

Moonen, P., V. Dorer, and J. Carmeliet, 2011: Evaluation of the ventilation potential of courtyards and urban street canyons using RANS and LES. *Journal of Wind Engineering and Industrial Aerodynamics*, **99 (4)**, 414

– 423, doi:http://dx.doi.org/10.1016/j.jweia.2010.12.012, URL http://www.sciencedirect.com/science/article/pii/S0167610510001455, the Fifth International Symposium on Computational Wind Engineering.

Muraoka, H., and Coauthors, 2010: Effects of seasonal and interannual variations in leaf photosynthesis and canopy leaf area index on gross primary production of a cool-temperate deciduous broadleaf forest in takayama, japan. *Journal of Plant Research*, **123 (4)**, 563–576, doi:10.1007/s10265-009-0270-4, URL http://dx.doi.org/10.1007/s10265-009-0270-4.

Nosek, Š., L. Kukačka, R. Kellnerová, K. Jurčáková, and Z. Jaňour, 2016: Ventilation processes in a three-dimensional street canyon. *Boundary-Layer Meteorology*, **159 (2)**, 259–284, doi:10.1007/s10546-016-0132-2, URL http://dx.doi.org/10.1007/s10546-016-0132-2.

Nozu, T., T. Tamura, Y. Okuda, and S. Sanada, 2008: LES of the flow and building wall pressures in the center of tokyo. *Journal of Wind Engineering and Industrial Aerodynamics*, **96 (10–11)**, 1762 – 1773, doi:http://dx.doi.org/10.1016/j.jweia.2008.02.028, URL http://www.sciencedirect.com/science/article/pii/S0167610508000457, 4th International Symposium on Computational Wind Engineering (CWE2006).

Oke, T., 1973: City size and the urban heat island. *Atmospheric Environment (1967)*, **7 (8)**, 769 – 779, doi:http://dx.doi.org/10.1016/0004-6981(73)90140-6, URL http://www.sciencedirect.com/science/article/pii/0004698173901406.

Oke, T., 1988: Street design and urban canopy layer climate. *Energy and Buildings*, **11 (1)**, 103–113.

Oke, T., 2006: *Initial Guidance to Obtain Representative Meteorological Observations at Urban Sites*. Intruments and Observing Methods. Report no. 81, World Meteorological Organization, URL https://books.google.fi/books?id=uJkznQEACAAJ.

Oke, T. R., 1987: *Boundary layer climates, 2nd edn.* Routledge, London.

Ossanlis, I., P. Barmpas, and N. Moussiopoulos, 2007: *The Effect of the Street Canyon Length on the Street Scale Flow Field and Air Quality: A Numerical Study*, 632–640. Springer US, Boston, MA, doi:10.1007/978-0-387-68854-1_67, URL http://dx.doi.org/10.1007/978-0-387-68854-1_67.

Padilla-Marcos, M. A., J. Feijó-Muñoz, and A. Meiss, 2016: Wind velocity effects on the quality and efficiency of ventilation in the modelling of outdoor spaces.

Case studies. *Building Services Engineering Research and Technology*, **37 (1)**, 33–50, doi:10.1177/0143624415596441, URL http://bse.sagepub.com/content/37/1/33.abstract.

PALM, 2016: The PALM tutorial. URL https://palm.muk.uni-hannover.de/trac/wiki/doc/tut, [Online. Accessed Feb 2016], Leibniz Universität Hannover.

Park, S.-B., J.-J. Baik, and B.-S. Han, 2015a: Large-eddy simulation of turbulent flow in a densely built-up urban area. *Environmental Fluid Mechanics*, **15 (2)**, 235–250.

Park, S.-B., J.-J. Baik, and S.-H. Lee, 2015b: Impacts of mesoscale wind on turbulent flow and ventilation in a densely built-up urban area. *Journal of Applied Meteorology and Climatology*, **54 (4)**, 811–824, doi:10.1175/JAMC-D-14-0044.1, URL http://dx.doi.org/10.1175/JAMC-D-14-0044.1.

Pirinen, P., H. Simola, J. Allto, J.-P. Kaukoranta, P. Karlsson, and R. Ruuhela, 2012: *Climatological statistics of Finland 1981–2010*. Finnish Meteorological Institute, Erik Palménin auko 1, P.O. Box 503, FIN-00101 Helsinki, Finland.

Pope, C. A. I., and D. W. Dockery, 2006: Health effects of fine particulate air pollution: Lines that connect. *Journal of the air & waste management association*, **56 (6)**, 709–742.

Pope, S., 2000: *Turbulent Flows*. Cambridge University Press, URL https://books.google.fi/books?id=4rghAwAAQBAJ.

Pugh, T. A. M., A. R. MacKenzie, J. D. Whyatt, and C. N. Hewitt, 2012: Effectiveness of green infrastructure for improvement of air quality in urban street canyons. *Environmental Science & Technology*, **46 (14)**, 7692–7699, doi:10.1021/es300826w, URL http://dx.doi.org/10.1021/es300826w, pMID: 22663154.

Ramponi, R., B. Blocken, L. B. de Coo, and W. D. Janssen, 2015: CFD simulation of outdoor ventilation of generic urban configurations with different urban densities and equal and unequal street widths. *Building and Environment*, **92**, 152 – 166, doi:http://dx.doi.org/10.1016/j.buildenv.2015.04.018, URL http://www.sciencedirect.com/science/article/pii/S0360132315001845.

Raupach, M. R., J. J. Finnigan, and Y. Brunet, 1996: *Boundary-Layer Meteorology 25th Anniversary Volume, 1970–1995: Invited Reviews and Selected Contributions to Recognise Ted Munn's Contribution as Editor over the Past 25 Years*, chap. Coherent Eddies and Turbulence in Vegetation Canopies: The

Mixing-Layer Analogy, 351–382. Springer Netherlands, Dordrecht, doi:10.1007/978-94-017-0944-6_15, URL http://dx.doi.org/10.1007/978-94-017-0944-6_15.

Razak, A. A., A. Hagishima, N. Ikegaya, and J. Tanimoto, 2013: Analysis of airflow over building arrays for assessment of urban wind environment. *Building and Environment*, **59**, 56 – 65, doi:http://dx.doi.org/10.1016/j.buildenv.2012.08.007, URL http://www.sciencedirect.com/science/article/pii/S0360132312002090.

Reynolds, O., 1895: On the dynamical theory of incompressible viscous fluids and the determination of the criterion. *Philosophical Transactions of the Royal Society of London A: Mathematical, Physical and Engineering Sciences*, **186**, 123–164, doi:10.1098/rsta.1895.0004, URL http://rsta.royalsocietypublishing.org/content/186/123, http://rsta.royalsocietypublishing.org/content/186/123.full.pdf.

Riikonen, A., L. Järvi, and E. Nikinmaa, 2016: Environmental and crown related factors affecting street tree transpiration in Helsinki, Finland. *Urban Ecosystems*, 1–23, doi:10.1007/s11252-016-0561-1, URL http://dx.doi.org/10.1007/s11252-016-0561-1.

Sagaut, P., 2006: *Large Eddy Simulation for Incompressible Flows: An Introduction*. Scientific Computation, Springer, URL https://books.google.fr/books?id=ODYiH6RNyoQC.

Salim, M. H., K. H. Schlünzen, and D. Grawe, 2015: Including trees in the numerical simulations of the wind flow in urban areas: Should we care? *Journal of Wind Engineering and Industrial Aerodynamics*, **144**, 84 – 95, doi:http://dx.doi.org/10.1016/j.jweia.2015.05.004, URL http://www.sciencedirect.com/science/article/pii/S0167610515001178, selected papers from the 6th International Symposium on Computational Wind Engineering {CWE} 2014.

Salim, S., R. Buccolieri, A. Chan, S. D. Sabatino, and S. Cheah, 2011a: Urban environmental pollution 2010: Large eddy simulation of the aerodynamic effects of trees on pollutant concentrations in street canyons. *Procedia Environmental Sciences*, **4**, 17 – 24, doi:http://dx.doi.org/10.1016/j.proenv.2011.03.003, URL http://www.sciencedirect.com/science/article/pii/S1878029611000296.

Salim, S. M., S. C. Cheah, and A. Chan, 2011b: Numerical simulation of dispersion in urban street canyons with avenue-like tree plantings: Comparison between RANS and LES. *Building and Environment*, **46 (9)**, 1735 – 1746, doi:http://dx.doi.org/10.1016/j.buildenv.2011.01.032, URL http://www.sciencedirect.com/science/article/pii/S0360132311000710.

Souch, C., and S. Grimmond, 2006: Applied climatology: urban climate. *Progress in Physical Geography*, **30 (2)**, 270–279, URL http://search.proquest.com/docview/231091259?accountid=11365.

Steinfeld, G., S. Raasch, and T. Markkanen, 2008: Footprints in homogeneously and heterogeneously driven boundary layers derived from a Lagrangian stochastic particle model embedded into large-eddy simulation. *Boundary-Layer Meteorology*, **129 (2)**, 225–248.

Stull, R. B., 1988: *An Introduction to Boundary Layer Meteorology*. Springer Netherlands, Dordrecht, 1–27 pp., doi:10.1007/978-94-009-3027-8_1, URL http://dx.doi.org/10.1007/978-94-009-3027-8_1.

Tamura, T., 2008: Towards practical use of LES in wind engineering. *Journal of Wind Engineering and Industrial Aerodynamics*, **96 (10–11)**, 1451 – 1471, doi:http://dx.doi.org/10.1016/j.jweia.2008.02.034, URL http://www.sciencedirect.com/science/article/pii/S0167610508000263, 4th International Symposium on Computational Wind Engineering (CWE2006).

Thaker, P., and S. Gokhale, 2016: The impact of traffic-flow patterns on air quality in urban street canyons. *Environmental Pollution*, **208, Part A**, 161 – 169, doi:http://dx.doi.org/10.1016/j.envpol.2015.09.004, URL http://www.sciencedirect.com/science/article/pii/S026974911530052X, special Issue: Urban Health and Wellbeing.

Tomas, J. M., M. J. B. M. Pourquie, and H. J. J. Jonker, 2016: Stable stratification effects on flow and pollutant dispersion in boundary layers entering a generic urban environment. *Boundary-Layer Meteorology*, **159 (2)**, 221–239, doi:10.1007/s10546-015-0124-7, URL http://dx.doi.org/10.1007/s10546-015-0124-7.

Tominaga, Y., and T. Stathopoulos, 2011: CFD modeling of pollution dispersion in a street canyon: Comparison between LES and RANS. *Journal of Wind Engineering and Industrial Aerodynamics*, **99 (4)**, 340 – 348, doi:http://dx.doi.org/10.1016/j.jweia.2010.12.005, URL http://www.sciencedirect.com/science/article/pii/S0167610510001388, the Fifth International Symposium on Computational Wind Engineering.

Tominaga, Y., and T. Stathopoulos, 2013: CFD simulation of near-field pollutant dispersion in the urban environment: A review of current modeling techniques. *Atmospheric Environment*, **79**, 716 – 730, doi:http://dx.doi.org/10.1016/j.atmosenv.2013.07.028, URL http://www.sciencedirect.com/science/article/pii/S1352231013005499.

United Nations, 2014: Urban and rural areas 2014. URL http://esa.un.org/unpd/wup/Wallcharts/WUP_2014%20Urban-Rural%20Areas%20Wallchart.pdf, Department of Economic and Social Affairs, Population Division 2014.

Vardoulakis, S., B. E. Fisher, K. Pericleous, and N. Gonzalez-Flesca, 2003: Modelling air quality in street canyons: a review. *Atmospheric Environment*, **37 (2)**, 155 – 182, doi:http://dx.doi.org/10.1016/S1352-2310(02)00857-9, URL http://www.sciencedirect.com/science/article/pii/S1352231002008579.

Vos, P. E., B. Maiheu, J. Vankerkom, and S. Janssen, 2013: Improving local air quality in cities: To tree or not to tree? *Environmental Pollution*, **183**, 113 – 122, doi:http://dx.doi.org/10.1016/j.envpol.2012.10.021, URL http://www.sciencedirect.com/science/article/pii/S0269749112004605, selected Papers from Urban Environmental Pollution 2012.

Walton, A., and A. Cheng, 2002: Large-eddy simulation of pollution dispersion in an urban street canyon—Part II: idealised canyon simulation. *Atmospheric Environment*, **36 (22)**, 3615 – 3627, doi:http://dx.doi.org/10.1016/S1352-2310(02)00260-1, URL http://www.sciencedirect.com/science/article/pii/S1352231002002601.

Weil, J. C., P. P. Sullivan, and C. H. Moeng, 2004: The use of large-eddy simulations in Lagrangian particle dispersion models. *Journal of the Atmospheric Sciences*, **61 (23)**, 2877–2887.

Weschler, C. J., and H. C. Shields, 2000: The influence of ventilation on reactions among indoor pollutants: Modeling and experimental observations. *Indoor Air*, **10 (2)**, 92–100, doi:10.1034/j.1600-0668.2000.010002092.x, URL http://dx.doi.org/10.1034/j.1600-0668.2000.010002092.x.

WHO, 2012: Public health and environment. URL http://www.who.int/gho/phe/en/, [Online. Accessed 2 Mar 2016], Global Health Observatory (GHO) data.

Wicker, L., and W. Skamarock, 2002: Time-splitting methods for elastic models using forward time schemes. *Monthly Weather Review*, **130 (8)**, 2088–2097.

Xiaomin, X., H. Zhen, and W. Jiasong, 2006: The impact of urban street layout on local atmospheric environment. *Building and Environment*, **41 (10)**, 1352 – 1363, doi:http://dx.doi.org/10.1016/j.buildenv.2005.05.028, URL http://www.sciencedirect.com/science/article/pii/S0360132305002003.

Xie, X., Z. Huang, J. Wang, and Z. Xie, 2005: The impact of solar radiation and street layout on pollutant dispersion in street canyon. *Building and Environment*, **40 (2)**, 201 – 212, doi:http://dx.doi.org/10.1016/j.buildenv.2004.07.013, URL http://www.sciencedirect.com/science/article/pii/S0360132304001763.

Xie, X., C.-H. Liu, and D. Y. Leung, 2007: Impact of building facades and ground heating on wind flow and pollutant transport in street canyons. *Atmospheric Environment*, **41 (39)**, 9030 – 9049, doi:http://dx.doi.org/10.1016/j.atmosenv.2007.08.027, URL http://www.sciencedirect.com/science/article/pii/S1352231007007121.

Xie, Z.-T., and I. P. Castro, 2009: Large-eddy simulation for flow and dispersion in urban streets. *Atmospheric Environment*, **43 (13)**, 2174 – 2185, doi:http://dx.doi.org/10.1016/j.atmosenv.2009.01.016, URL http://www.sciencedirect.com/science/article/pii/S135223100900034X.

Yaghoobian, N., J. Kleissl, and K. T. U. Paw, 2014: An improved three-dimensional simulation of the diurnally varying street-canyon flow. *Boundary-Layer Meteorology*, **153 (2)**, 251–276.

Yang, F., Y. Gao, K. Zhong, and Y. Kang, 2016: Impacts of cross-ventilation on the air quality in street canyons with different building arrangements. *Building and Environment*, **104**, 1 – 12, doi:http://dx.doi.org/10.1016/j.buildenv.2016.04.013, URL http://www.sciencedirect.com/science/article/pii/S0360132316301342.

Yazid, A. W. M., N. A. C. Sidik, S. M. Salim, and K. M. Saqr, 2014: A review on the flow structure and pollutant dispersion in urban street canyons for urban planning strategies. *Simulation*, **90 (8)**, 892–916, doi:10.1177/0037549714528046, URL http://dx.doi.org/10.1177/0037549714528046.

Zheng, Y., Y. Miao, S. Liu, B. Chen, H. Zheng, , and S. Wang, 2015: Simulating flow and dispersion by using WRF-CFD coupled model in a built-up area of Shenyang, China. *Advances in Meteorology*, **2015**.